






Article

Load versus Strain Relationships of Single and Continuous Span Full-Scale Pre-cast Prestressed Concrete Girders for Monorail Systems

Suniti Suparp ¹, Athasit Sirisonthi ², Nazam Ali ³, Noha Saad ⁴, Krisada Chaiyasarn ⁵, Marc Azab ⁴, Panuwat Joyklad ^{1,*} and Qudeer Hussain ⁶

¹ Department of Civil and Environmental Engineering, Faculty of Engineering, Srinakharinwirot University, Nakhonnayok 26120, Thailand

² Sino-Thai Engineering & Construction Public Company Limited, Bangkok 10330, Thailand

³ Department of Civil Engineering, School of Engineering, University of Management and Technology, Lahore 54770, Pakistan

⁴ College of Engineering and Technology, American University of the Middle East, Egaila 54200, Kuwait

⁵ Thammasat Research Unit in Infrastructure Inspection and Monitoring, Repair and Strengthening (IIMRS), Thammasat School of Engineering, Faculty of Engineering, Thammasat University Rangsit, Pathumthani 12000, Thailand

⁶ Center of Excellence in Earthquake Engineering and Vibration, Department of Civil Engineering, Chulalongkorn University, Bangkok 10330, Thailand

* Correspondence: panuwatj@g.swu.ac.th



Citation: Suparp, S.; Sirisonthi, A.; Ali, N.; Saad, N.; Chaiyasarn, K.; Azab, M.; Joyklad, P.; Hussain, Q. Load versus Strain Relationships of Single and Continuous Span Full-Scale Pre-cast Prestressed Concrete Girders for Monorail Systems. *Buildings* **2022**, *12*, 1164. <https://doi.org/10.3390/buildings12081164>

Academic Editors: Chunxu Qu, Shibin Lin, Donghui Yang and Sadegh Shams

Received: 22 June 2022

Accepted: 26 July 2022

Published: 4 August 2022

Publisher's Note: MDPI stays neutral with regard to jurisdictional claims in published maps and institutional affiliations.



Copyright: © 2022 by the authors. Licensee MDPI, Basel, Switzerland. This article is an open access article distributed under the terms and conditions of the Creative Commons Attribution (CC BY) license (<https://creativecommons.org/licenses/by/4.0/>).

Abstract: Full-scale testing of multiple span girders is scarce in the literature, often related to the complexity of loading setup and time constraints. The importance of full-scale tests is manifested in the fact that useful information regarding failure mechanisms can be obtained. In addition, important guidelines can be established for structural designers. Further, results from full-scale tests can help establish constitutive laws for various mechanisms involved in the response of actual structures. The structural performance of individual members can be assessed by monitoring their strains at service and ultimate loads. This study presents a comparison of experimentally monitored strains on longitudinal steel bars, stirrups, and prestressing tendons embedded in single and multi-span full-scale precast pre-tensioned girders. These girders were constructed and detailed to simulate the response of newly proposed straddle-type monorail girders. Single-span girders were tested under monotonic two-point service and ultimate loads, whereas multi-span girders were tested under both two- and four-point service and ultimate load. It was revealed that longitudinal steel and prestressing tendon strains monitored within single-span girders at service and ultimate loads were significantly higher than those recorded at corresponding locations in multi-span girders.

Keywords: modern cities; monorail system; full-scale precast post-tension girder; service load; ultimate load; straddle monorail

1. Introduction

The rapid growth of modern cities confronts existing infrastructure capabilities, with particular emphasis on the construction of new public facilities. The monorail transportation system has evolved in recent times to be an excellent measure to tackle these challenges. Monorails are widely adopted for small to medium cities [1,2], attributed to their advantages, such as low noise, rapid construction, and efficient climbing abilities [3]. A monorail can be constructed either in straddle or suspension form [4].

Bangkok is the capital of Thailand. It has enticed millions of people in recent times and its neighborhoods have expanded swiftly. This has challenged the concerned authorities to meet the growing need for additional infrastructure required in a limited time. Recently, the Mass Rapid Transit Authority (MRTA) chose monorail systems to meet these demands. The

construction of a monorail system in Bangkok was granted to BSR, which is a joint venture among BTS, Sino-Thai Engineering and Construction Public Company Limited (STECON), and RATCH Group Public Company Limited, Thailand. Later, STECON received the rights to be the exclusive contractor and proposed a novel four-span Post-Tensioned Girder System (PTGS), including four guideway beams (GWBs), post-tensioned with tendons running through four consecutive spans.

The importance of full-scale tests is manifested in the fact that useful information regarding failure mechanisms can be obtained. In addition, important guidelines can be recognized by structural designers. Further, results from the full scale can help establish constitutive laws for various mechanisms involved in the response of actual structures. This can help to perform more realistic non-linear finite element modelling in the context of the performance-based assessment of structures. To date, information regarding full-scale tests of bridge girders and decks is limited. Kim et al. [5] utilized sequential vibration-impedance approaches to detect tendon and girder damage in two prestressed concrete bridges. By using the measured acceleration records, modal characteristics of the bridges were extracted and frequency- and mode shape-based methods were used to locate and estimate the extent of the damage. Ai et al. [6] proposed a numerical analysis scheme to detect concrete cracking and its growth in flexure-critical prestressed concrete structures using electro-mechanical admittance. Takebayashi et al. [7] carried out a full-scale test to investigate the behavior of the precast segmental box girder bridge. A full-scale 45 m deck was constructed and tested until failure. It was concluded that the maximum moment resisted by the bridge was 18% higher than its nominal moment capacity. This conclusion demonstrated the adequacy of the design. Labia et al. [8] carried out an experimental program comprising the testing of two full-scale precast pre-tensioned box girders. The total length of the girders was approximately 21.34 m. A monotonic load was applied till the failure and strain profiles, cracks, and deflections were monitored. Experimental ultimate moment and prestress loss were compared with different code provisions. Good agreement between experimental and code-predicted ultimate loads was found. However, a significant disparity between the predicted and experimental ductility and prestress loss was found. Graybeal [9] assessed the flexural performance of a full-scale ultra-high-performance concrete I girder. A 193 MPa steel-fiber-reinforced concrete section was utilized to construct a 24.4 m long girder comprising 26 prestressing strands. Various response parameters, including strain profiles, flexural stiffness, moment capacity, and cracks, were monitored. Centered on their results, a design philosophy for this type of bridge was proposed. To replace conventional steel with carbon-fiber-reinforced polymer (CFRP) to avoid corrosion-induced deterioration, Grace et al. [10] conducted experimental tests on 1/3rd scale AASHTO-type prestressed concrete beam bridges. Response parameters were monitored under both service and ultimate load limits, with the load being applied through a 4-point load spreader. Inherently, composite materials remain elastic until their ultimate point. To avoid brittle behavior, CFRP bars were distributed along the depth of the girder. For a single layer of CFRP bars, a brittle failure was reported. On the contrary, the bridge behaved in a ductile manner with distributed CFRP bar layers. Leeuwen and Adebar [11] performed a full-scale test on a 17.1 m long hybrid bridge girder comprising reinforced concrete web and steel flanges. Behavior was monitored both at service and ultimate loads. Well-confined and small cracks were reported under the service load. At ultimate load, diagonal cracks were reported within the web. However, the ultimate response was controlled by flexure. In addition to experimental studies, some studies [12,13] also reported finite element analysis of full-scale box girder bridges.

More recently, authors [14] conducted an experimental study to investigate the response of a three-span full-scale precast pre-tensioned continuous (FPPC) girder for the proposed monorail system described earlier. Each girder was approximately 30 m long and incorporated with the actual design of the proposed straddle-type monorail system. The girder was subjected to two-point service, four-point service, and four-point ultimate loads. The elastic response was observed under service loads with minimal cracking. Observed de-

flections were smaller than those allowed by the code provisions. Under the ultimate load, load capacity was found to be higher than the design capacity, proving the appropriateness of the structural design. Experimental tests and finite element analysis of a single-span full-scale precast pre-tensioned (FPP) girder were carried out by authors [15]. Dimensions and structural details of the girder resembled the interior girder of the three-span FPPC girder tested by authors [14], as both the girders were expected to dominate in flexure. Ultimate load and deflections of the tested FPP girder were found within the code limits and nominal capacities.

Full-scale testing of multiple-span girders is scarce in the literature, often related to the complexity of loading setup and time constraints. The structural performance of individual members can be assessed by monitoring their strains at service and ultimate loads. This study focuses on the comparison of reinforcement steel strains (longitudinal, stirrups, and tendons) in full-scale multiple-span and single-span precast pre-tensioned girders under service and ultimate loads.

To date, no direct study is available to compare the steel bar strain response of single and continuous precast post-tensioned girders. This is important in the sense that single girders with similar geometrical and structural details are tested to assess the performance of similar girders in a continuous girder system. The present study finds that within service limits of the applied load, longitudinal steel strains in single girders were higher than those in continuous girders measured at similar locations. This trend was observed for the case of ultimate loads as well. A similar discrepancy was also observed in the case of stirrup and tendon strains, explaining that a single-span girder with similar geometrical and structural details as that of a span in a continuous girder system cannot approximate the structural response of the latter.

2. Construction Details of Girder Specimens

Three different full-scale precast post-tensioned (FPP) girder specimens were tested. Considered girders simulated the actual design, size, and construction details of the girders for the newly proposed straddle monorail system. One of the specimens (SP-1) contained three reinforced concrete (RC) hollow haunched girders, two pier segments, four piers, four wet joints, and four bearings at each support, as shown in Figure 1. Two of the exterior spans simulated the response of exterior girders, while the middle span mimicked an interior span. Right and left exterior spans were 30.65 and 31.4 m, respectively. Both the exterior spans were constructed with similar construction details. Cross-sectional dimensions of the girders at the ends were 690×2000 mm, which were gradually haunched to achieve a cross-section of 690×1600 mm at its mid span. The size of the hollow opening in the middle of the girders was 270×1100 mm. The Interior girder had a total length of 30 m, with sectional details similar to those of the exterior girders. Internal supports were achieved through a combination of wet joints and pier segments, while girders were directly supported on external piers/supports. Each pier segment was $1000 \times 690 \times 2000$ mm (length \times width \times height). The increased bond strength between wet joints and pier segments was achieved by means of special shear keys. The empty space between girders and pier segments was grouted with a high-strength non-shrink cement grout to attain a wet joint of 20 cm in length. However, its width and depth were kept identical to those of the adjacent girders. Bearings were provided between each pier segment and its underneath pier. The second specimen SP-2 replicated the cross-sectional and reinforcement details of the interior girder of specimen SP-1. There were no wet joints provided and SP-2 rested directly onto pier segments. Similar to girders, pier segments, bearings, and piers were also identical to those provided in specimen SP-1. The third specimen SP-3 was intended to simulate the response of the exterior girders of specimen SP-1, with similar construction and reinforcement details, as well as identical support details. Further details of cross-sections, reinforcement, and post-tension tendons (PT) can be found in previous studies [14,15].

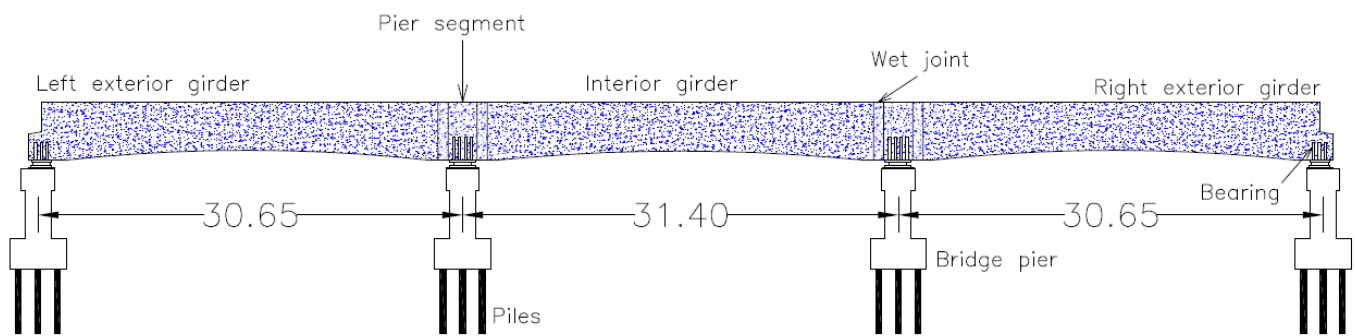


Figure 1. Typical details of test specimen (SP-1).

The continuity of the specimen SP-1 was accomplished by means of four post-tensioned tendons (T1, T2, T3, and T4), as shown in Figure 2. In addition to this, short tendons T5 and T6 were also provided with a bifold purpose: to achieve a connection between exterior and interior girders and to resist negative moments at the interior supports. Proper placement and alignment of post-tensioned tendons were accomplished using special-purpose steel plates and grips, as depicted in Figures 3 and 4.

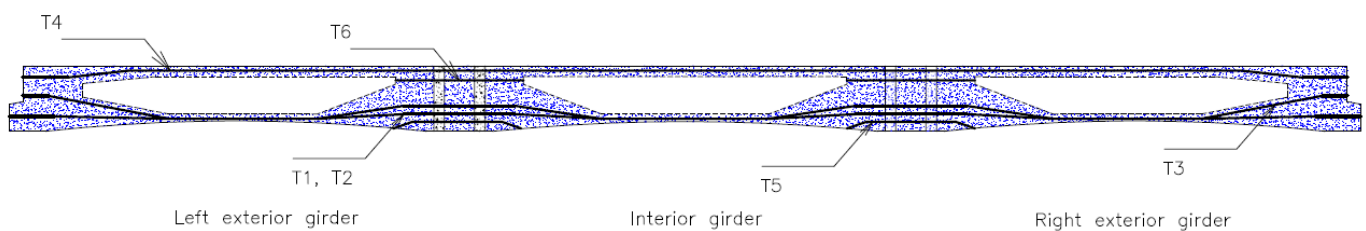


Figure 2. Details of post-tension tendons.



Figure 3. Anchorage for T6.



Figure 4. Application of tension to the PT tendons.

3. Material Properties

All components in each specimen were constructed using high-strength ready-mixed concrete. Concrete cylinders of dimensions 150 mm × 300 mm were cast to determine the compressive strength of the concrete, as per the recommendations of ASTM C39/C39M–21 [16]. Mix proportions of the concrete are given in Table 1, while average values of compressive strength for each component are presented in Table 2. All the reinforcement comprised deformed steel bars. Mechanical properties of the deformed steel bars for each size were evaluated as per the provisions of ASTM A615/A615M [17]. Table 3 enlists the yield and tensile strengths of the steel bars. Post-tensioned ducts were filled with a special cement grout whose properties were evaluated by performing compressive tests on standardized 50 × 50 mm cubes, as per ASTM C109/C109M–21 [18]. Table 2 also presents the compressive strength of the cement grout.

Table 1. Mix proportions of concrete.

Ingredients	Cement	Aggregate		Water
		Fine	Coarse	
Quantity kg/m ³	380	710	1100	210

Table 2. Compressive strengths of individual components.

Components	Compressive Strength (MPa)
Cement grout	45
Pier segment	62
Left exterior girder	65
Right exterior girder	64
Interior girder	65

Table 3. Mechanical properties of steel reinforcement.

Reinforcement	Yield Strength (MPa)	Ultimate Strength (MPa)
DB16	420	480
DB20	420	520
DB25	440	560
7-wire strands	1500	1800

4. Preparation of Specimens

Construction of all three specimens was carried out in a similar manner. Therefore, this section summarizes the construction method for specimen SP-1 only. Both the construction and testing were carried out at the site of Sino-Thai Engineering and Construction Public Company Limited (STECOM), located in Saraburi Province, Thailand. A special steel formwork was prepared to achieve the haunching of the girders. The bottom arch of the girders was achieved by providing a bottom haunch at the middle of the formwork, as shown in Figure 5. A steel cage for reinforcement was prepared separately and placed in the formwork by means of a crane after its completion. Inside, the hollow section of the girders was accomplished by adding a special foam into the steel reinforcement. High-strength concrete was then poured into the formwork. Steel formwork was removed 12 h after concrete placement while curing was continued for 28 days in ambient conditions. It is to be mentioned that the construction of pier segments and piers was conducted parallel to the construction of girders. A total number of 4 and 12 foundations was constructed to support three girders of specimen SP-1 and reaction frame, respectively. For the specimens SP-2 and SP-3, two and four foundations were constructed for the single girder and reaction frame, respectively. All foundations consisted of precast piles driven into the ground using a pile hammer, as shown in Figure 6a. Pile caps were introduced at the top of piles to facilitate the load transfer from top to bottom (Figure 6b). In the case of foundations of reaction frames, steel bolts were embedded in pile caps to fix the reaction frame, as shown in Figure 6c. For the case of piers, a column, with height of 1000 mm, was constructed at the top of the pile cap to support pier segments. In this study, special-purpose bearings were used to connect girders of all test specimens, i.e., SP-1, SP-2 and SP-3. Two types of bearings, fixed and free bearings, were used, as shown in Figure 7. The function of both bearings is identical, except that movement in the transverse direction was restrained in fixed bearings. For specimen SP-1, fixed bearing was used only at one end for support and free bearings were provided at the remaining supports, whereas in the case of specimens SP-2 and SP-3, one fixed and one free bearing was used at end supports. Once foundation work was finished, piers and girders were installed and aligned accurately. Then, post-tensioning was performed after placing continuous stands through all girders. This step was not carried out for specimens SP-2 and SP-3. Finally, wet joints were constructed and post-tensioning ducts were filled with high-strength non-shrink cement grout.



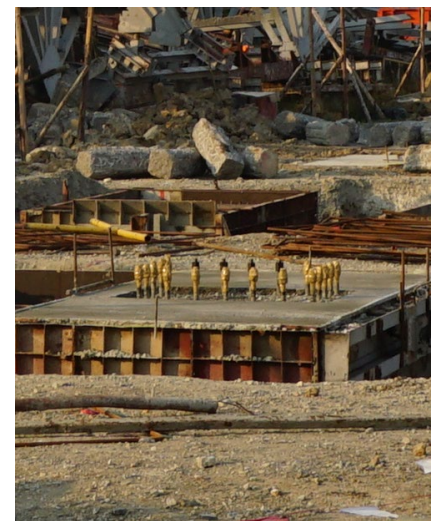
Figure 5. Typical view of formwork.



(a)

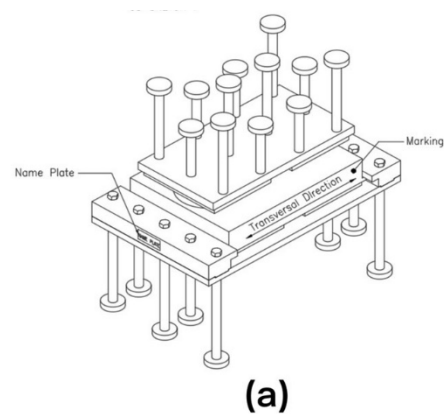


(b)

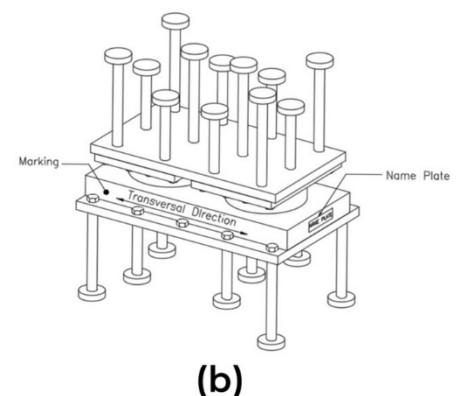


(c)

Figure 6. Construction details of foundations: (a) driving piles, (b) pile cap, and (c) steel bolts.



(a)



(b)

Figure 7. Details of bearing: (a) fixed bearing and (b) free bearing.

5. Instrumentation Details

In this study, strain gauges were installed on longitudinal steel bars, vertical stirrups (shear reinforcement), and post-tension (PT) tendons for each specimen at different locations. For specimen SP-1, the locations are graphically shown in Figure 8. The locations for both specimens, i.e., SP-2 and SP-3 are shown in Figure 9. In specimen SP-1, strain gauges for longitudinal steel bars (LG1) were installed at locations C1–C3 and E1–E12 (Figure 10), whereas in the case of specimens SP-2 and SP-3, strain gauges for longitudinal steel bars (LG1) were installed only at the middle of the span, i.e., C1. Further, at each location, four strain gauges (two strain gauges at top longitudinal and two strain gauges at bottom longitudinal steel bars) were installed, as shown in Figure 11a. The strain gauges at the top and bottom were recognized by the letters “T” and “B”, respectively. At the top and bottom, two strain gauges were used: one at the front side and one at the back. Therefore, the letters “F” and “K” were used to recognize strain gauges at the front and back, respectively. For instance, “TF” refers to the strain gauge on the front side of the top of the girder. The strain gauges (SG1) for vertical stirrups were installed at end locations of each girder in each specimen, i.e., D1–D6 and E1–12. Further, the strain gauge at the front side was referred to with letter F and strain gauge at the back side was referred to with K (Figure 11b). Further, to measure the strain of PT tendons, the strain gauges (TG1) were installed at PT tendons at different locations. In specimen SP-01, the strain gauges at PT tendons were installed at locations C1–C3, A2, and A3, whereas in specimens SP-2 and SP-3, strain gauges at PT tendons were installed only at the middle location C1. Although in this study, PT tendons comprised a 7-wire strand, only four strain gauges were installed due to their high cost, as shown in Figure 11c. It is pertinent to mention that in Figure 11a,b, XX shows the location of strain gauges, while in Figure 11c, XX also shows the location of the strain gauges. However, TX shows the number of PT tendons. These notations are represented for the convenience of the readers so that multiple repetitions can be avoided throughout the manuscript henceforth.

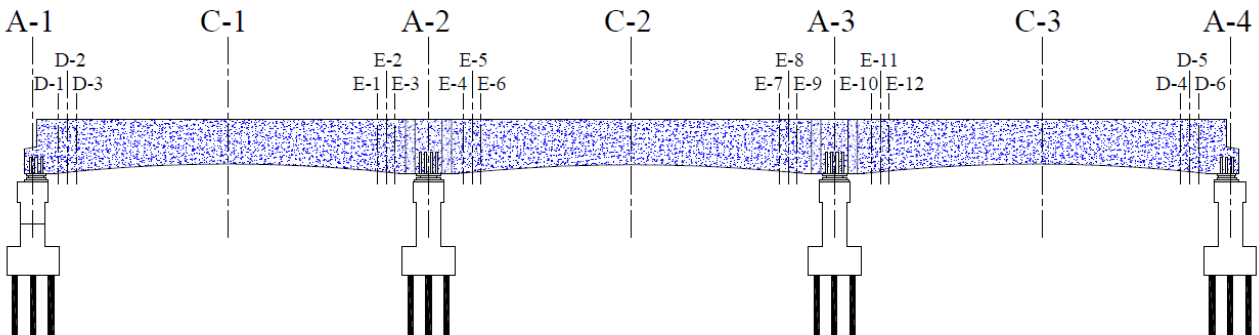


Figure 8. Details of locations for strain gauges (SP-1).

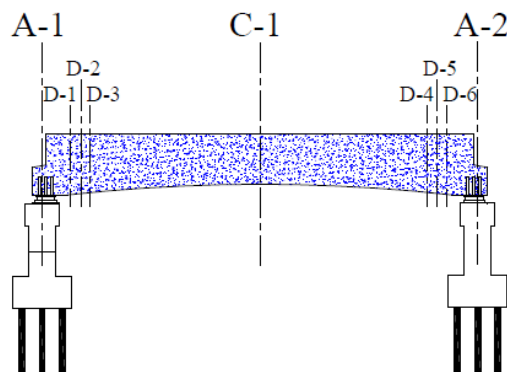


Figure 9. Details of locations for strain gauges (SP-2 and SP-3).

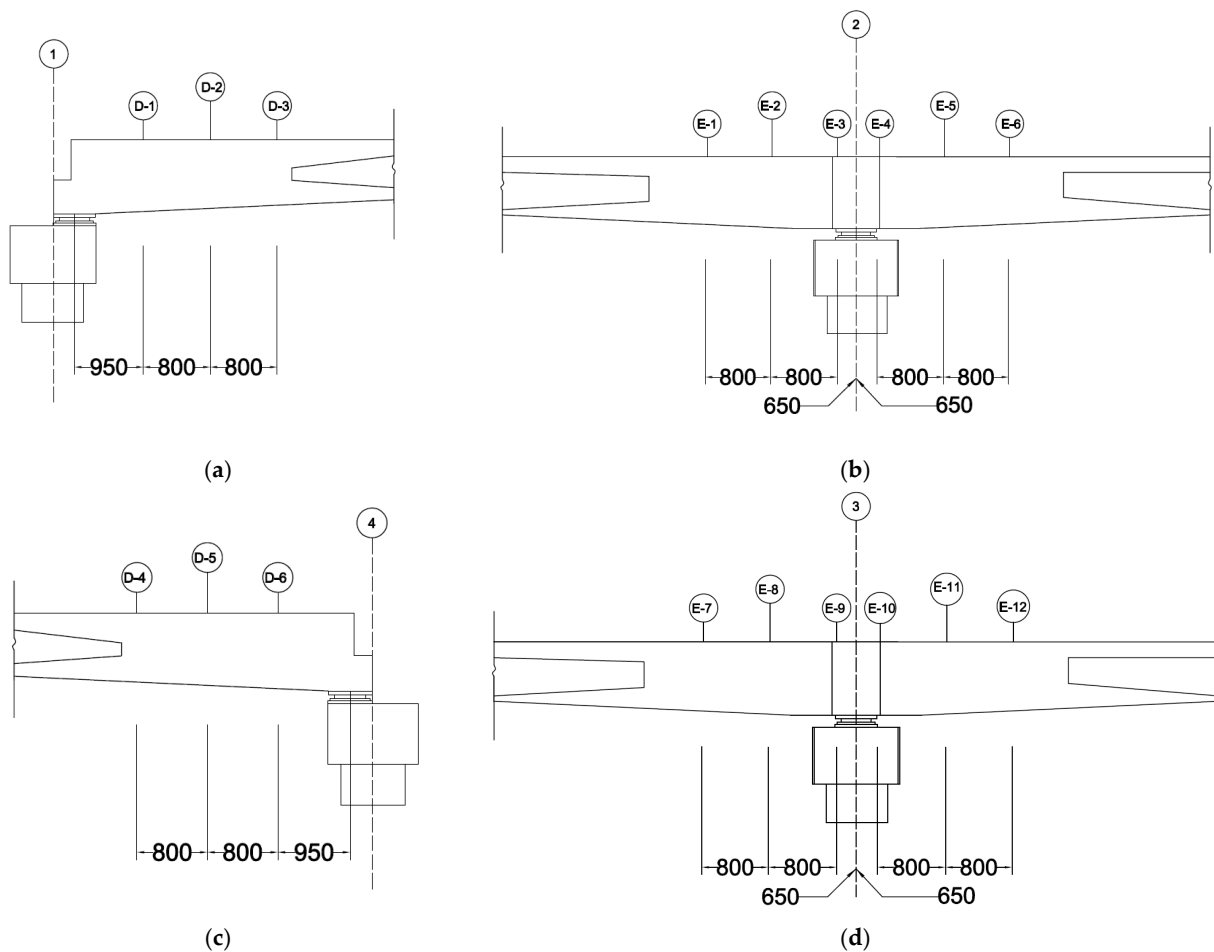


Figure 10. Details of end sections at locations (a) A-1, (b) A-2, (c) A-3 and (d) A-4 (units: mm).

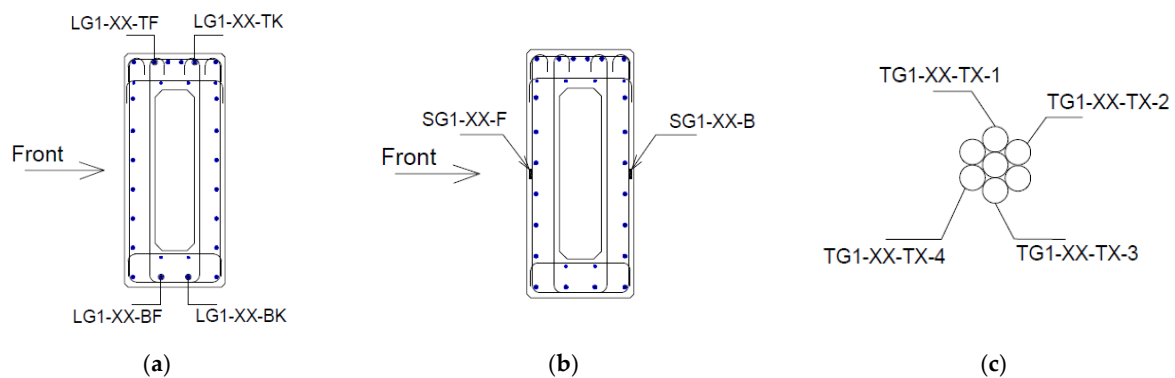


Figure 11. Details of strain gauges (a) LG1, (b) SG1, and (c) TG1.

6. Load Setup

Specimen SP-1 was subjected to four types of loadings to analyze its structural performance, both within serviceability and ultimate states. The first type of loading included a two-point load applied at the right exterior girder with a magnitude limited to the service limit. The second type of loading was also a two-point service load, but its point of application was the interior span. The third type of load was a four-point loading with magnitude limited to service load. However, the points of application were two points each on the left exterior and interior spans, as depicted in Figure 12. The last loading was similar to the third loading type. The only difference between the third- and fourth-point loading

was the magnitude of loading, which was increased to the ultimate state in the fourth type. Four types of loading setup will be referred to with SP-1-L01, SP-1-L02, SP-1-L03, and SP-1-L04 for the first, second, third, and fourth loading types. Loadings on specimens SP-2 and SP-3 were of two types. In the first type, a two-point load was applied up till the service limit, while it was increased to the ultimate state in the second type. It is worth mentioning that the service limit of the load was set corresponding to the onset of longitudinal steel bar strains, equivalent to 50% of their yield values. A two-point loading setup on specimen SP-2 is shown in Figure 13. Loading setups for specimen SP-2 are referred to with SP-2-L01 and SP-2-L02 for first and second loading types, respectively. Similarly, designations SP-3-L01 and SP-3-L03 are used for first and second loadings on specimen SP-3, respectively. A typical loading setup of specimen SP-3 is shown in Figure 14. Additional details on loading setups can be found in previous studies [14,15].



Figure 12. Typical load setup SP-1-L03 and SP-1-L04.



Figure 13. The two-point load applied to specimen SP-02.



Figure 14. The two-point load applied to specimen SP-02.

7. Experimental Results

7.1. Strain-Longitudinal Steel Bars

7.1.1. Specimen SP-1

Loading Setup SP-1-L01

This loading setup corresponds to the application of a two-point load at the right exterior span of specimen SP-1. As mentioned in earlier sections, four strain gauges were attached at each position along the longitudinal steel bars. However, the results presented here correspond only to the available data of strain recorded at each position and/or location. Positive values of strains are referred to as tension, while negative values are associated with compression. Therefore, positive values at supports showed strains at the top longitudinal bars, while positive values at midspan represented the response of bottom longitudinal bars. As shown in Figure 15a, the maximum tensile strain recorded was around 90 microns, while the maximum negative strain was around 140 microns. A similar response can also be observed in Figure 15b. At location C3, the maximum positive strain recorded was around 200 microns, while the corresponding negative value was 220 microns.

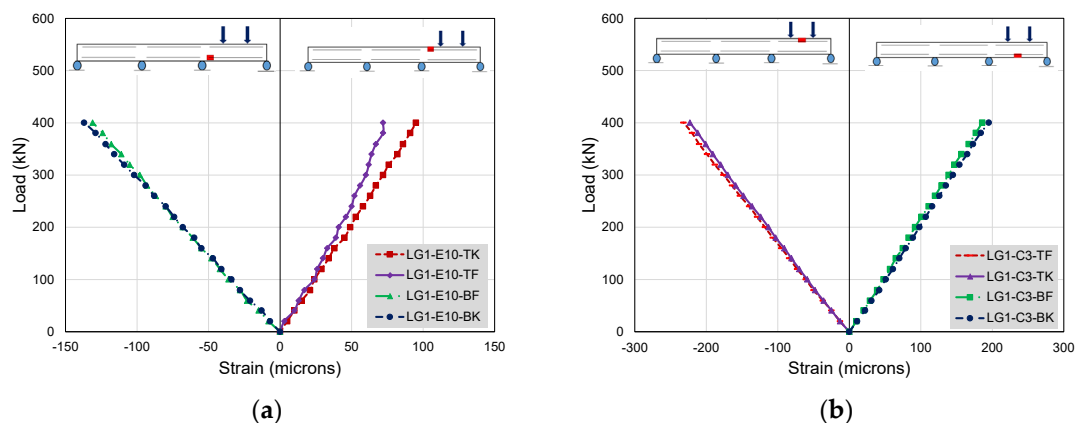


Figure 15. Strain versus load responses (a) location E10 and (b) location C3.

Loading Setup SP-1-L02

This loading setup refers to the application of a two-point load applied at the interior span of specimen SP-1. At locations E4–E6, the maximum positive and negative strains recorded were limited to 75 and 60 microns, respectively, as shown in Figure 16a. At

locations, E7–E9, Maximum positive and negative strains recorded under service loads were 95 and 72 microns, respectively (see Figure 16b). At location C2, both positive and negative strains reached 180–190 microns and were noticeably higher than those recorded at the interior faces of interior supports (Figure 16c).

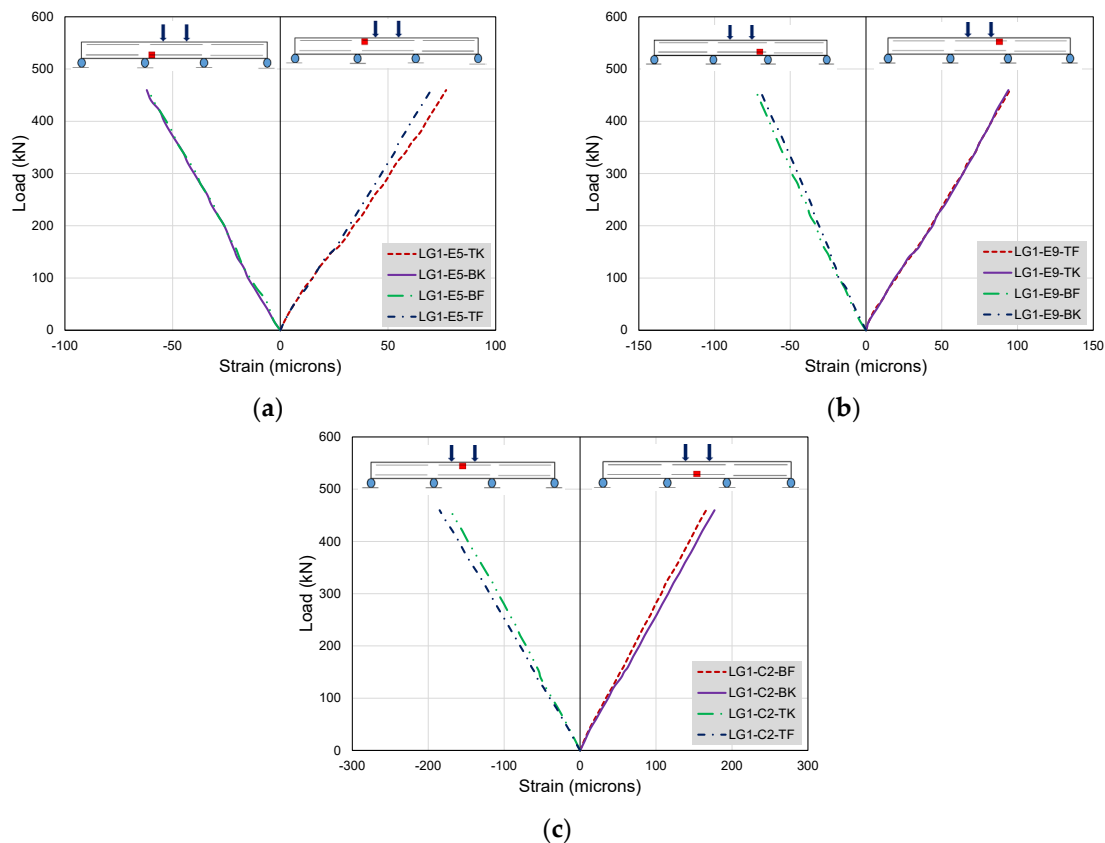


Figure 16. Strain versus load responses at locations (a) E5, (b) E9, and (c) C2.

Loading Setup SP-1-L03

This load corresponds to the application of a four-point service load at the interior and left exterior spans, as shown in Figure 12. In this loading setup, a linear relationship between load and strain was observed at all locations, as shown in Figure 17. At locations E1–E3 (exterior face of the left interior support), maximum positive and negative strains were approximately 120 microns, as shown in Figure 17a. At locations E4–E6, maximum positive and negative strains recorded at this position under four-point service load were limited to 105 and 110 microns, respectively, as shown in Figure 17b, whereas, at locations E7–E9, maximum strains recorded at this position were quite low, as compared to strains at other locations under the same load. Both positive and negative strains were limited to 50 microns (see Figure 17c), substantially lower than the yield strain. At location C1, maximum positive and negative strains were limited to 75 and 90 microns, respectively (see Figure 17d), under a four-point service load. At location C2, the maximum positive strain recorded at location C2 and under four-point service load was limited to 90 microns, while its corresponding negative recorded value was 105 microns, as shown in Figure 17e. It is worth mentioning that strain values recorded at this position and under two-point service loads were significantly higher, reaching around 190 microns.

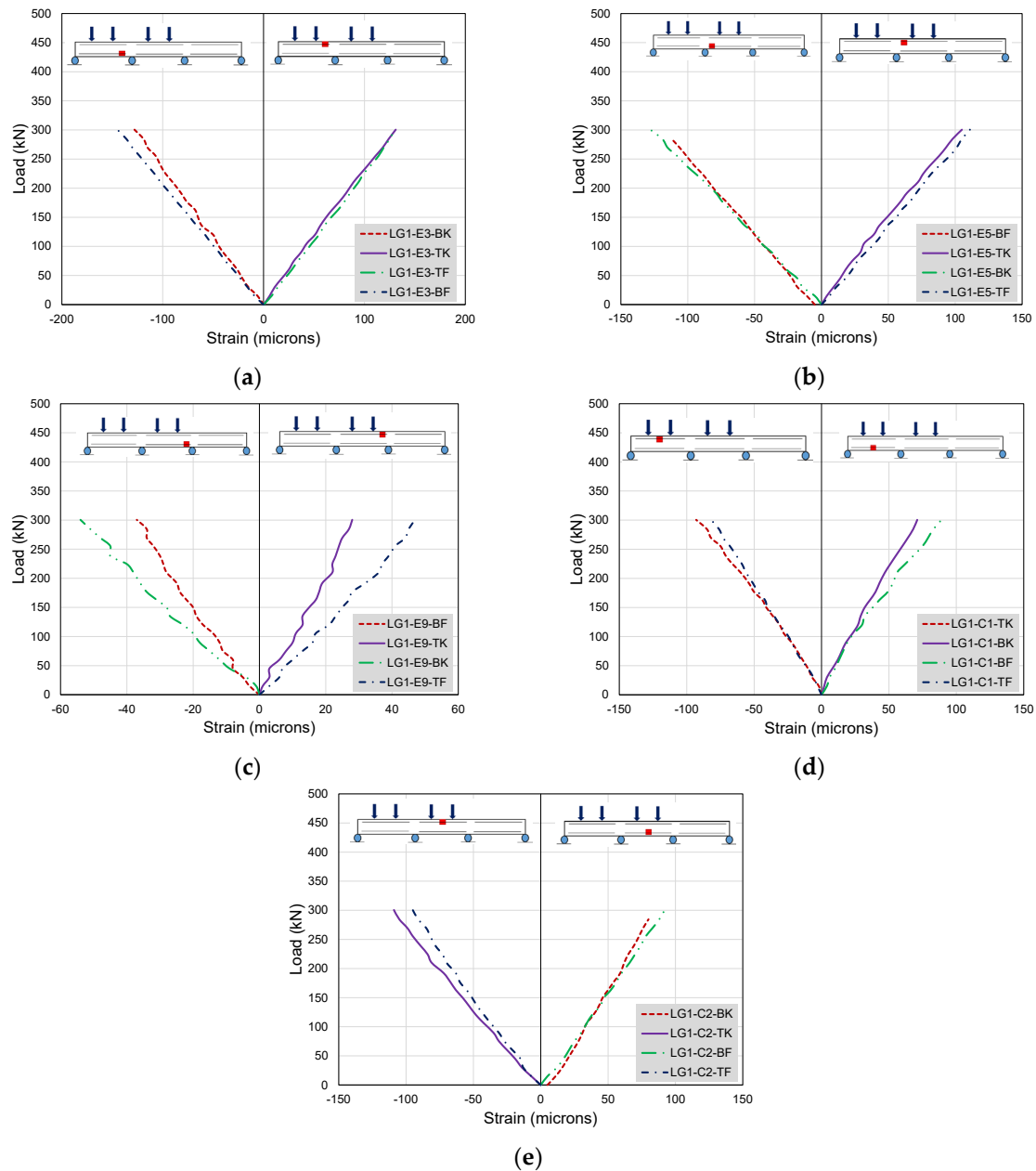


Figure 17. Strain versus load responses at locations (a) E3, (b) E5, and (c) E9, (d) C1, and (e) C2.

Loading Setup SP-1-L04

Under this setup, a four-point load was applied until the ultimate state to the interior and exterior spans of specimen SP-1 (Figure 12). At locations, E1–E3, the maximum positive strain recorded was around 1800 microns, which is less than the yield strain of steel bars. On the negative side, the maximum recorded strain was limited to 950 microns (see Figure 18a). At locations E4–E6, maximum positive and negative strains recorded at the interior face of the left interior supports were 1500 and 800 microns, respectively, as shown in Figure 18b. These strains were found to be significantly higher than those recorded under the same loading setup with load limited to service limits, whereas, at Locations E7–E9, maximum positive and negative strains recorded at the interior face of the right interior support were 200 and 350 microns, respectively, as shown in Figure 18c. At location C1, maximum strains obtained in both directions were limited to 750 microns, significantly lower than the yield strain (see Figure 18d). On the other hand, at location C2, the maximum positive recorded strain was lower than that recorded at location C1. However, the negative strain

achieved a similar value to that of its counterpart at location C1. As shown in Figure 18e, the strain–load relation remained linear and maximum recorded strains did not achieve the yield plateau. Maximum positive and negative strains recorded at this location and under four-point ultimate load were 500 and 750 microns, respectively.

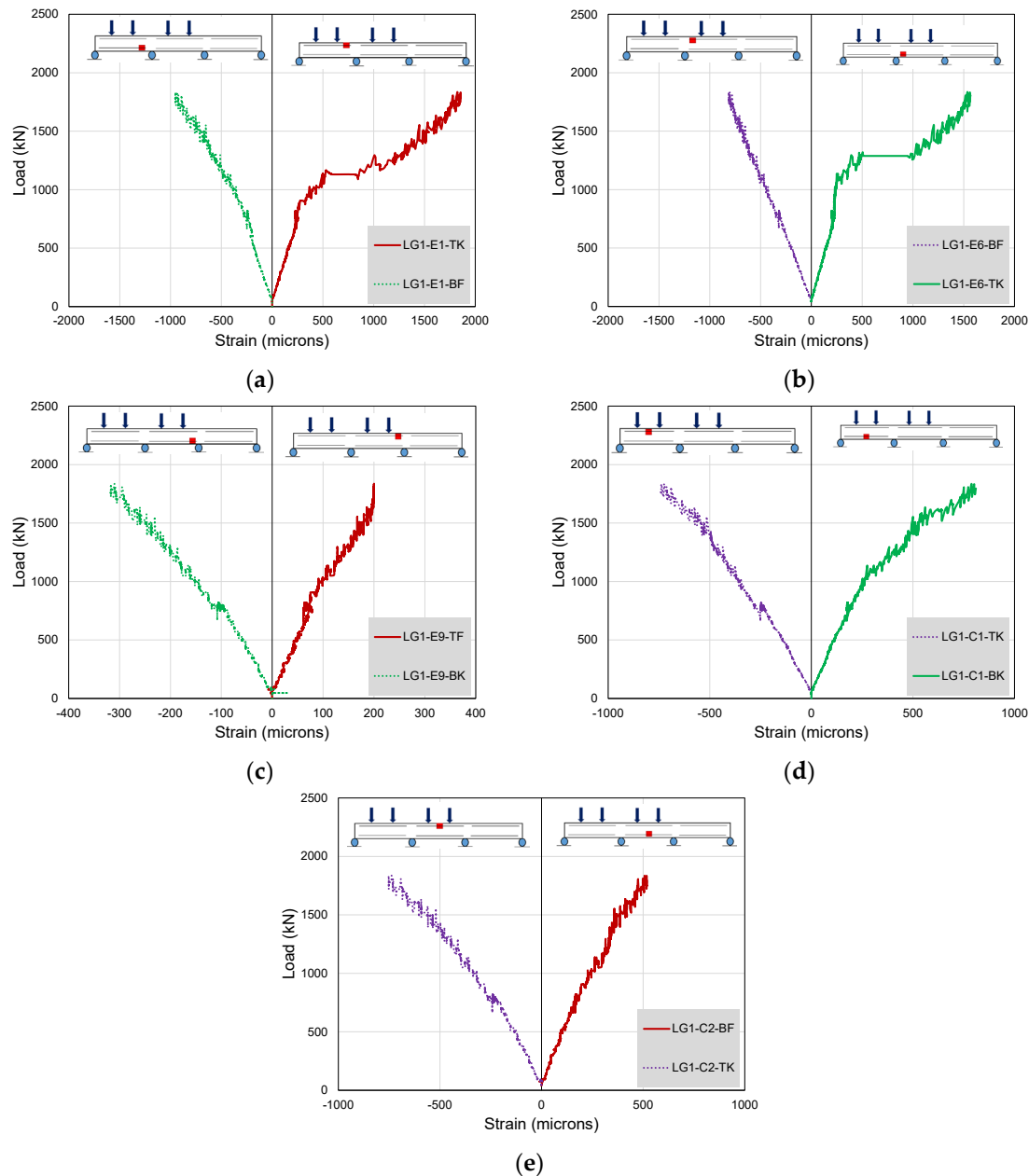


Figure 18. Strain versus load responses at locations (a) E1–E3, (b) E4–E6, and (c) E7–E9, (d) C1, and (e) C2.

7.1.2. Specimen SP-2

Specimen SP-2 was subjected to only two-point loading, but the magnitude of the applied load was varied; firstly, the magnitude of the load was limited to the service load (load setup SP-2-L01), where the definition of service load is the same as specified in earlier sections; secondly, the magnitude of the applied load was increased to the ultimate load (load setup SP-2-L02). In load setup SP-2-L01, the specimen SP-2 was a simply supported single-span girder. Since the moments were unrestrained at both ends, steel strains were only monitored at the mid span of specimen SP-2. Figure 19a presents the maximum

positive and negative strains recorded under this load setup. Maximum positive and negative strains recorded were 320 and 210 microns, respectively, while the load–strain relationship remained linear, whereas, in load setup SP-2-L02, the load setup was similar to SP-2-L01, with the difference being that the load was applied till the ultimate state. The maximum strain recorded was on the positive side, with a value of around 3000 microns. This value was beyond the yield strain of the bars. On the negative side, the maximum strain was limited to 2000 microns, as shown in Figure 19b.

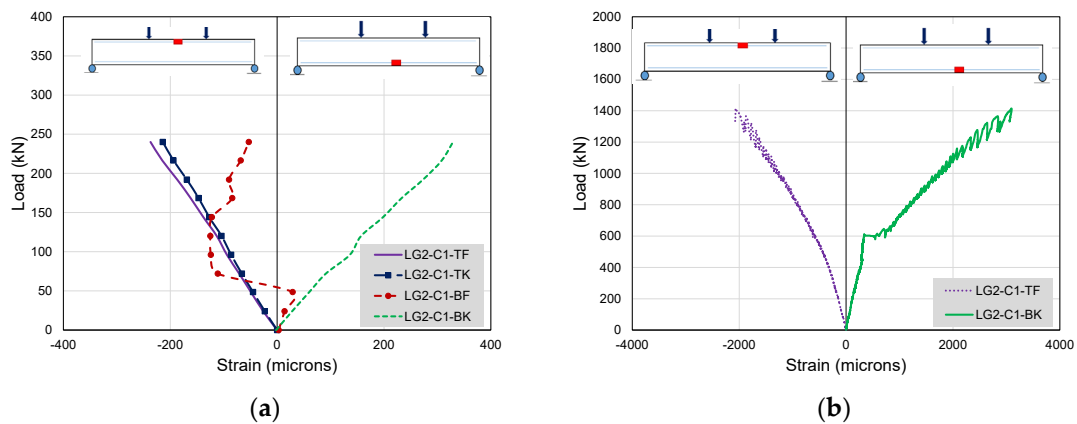


Figure 19. Strain versus load responses (a) load setup SP-2-L01 and (b) load setup SP-2-L02.

7.1.3. Specimen SP-3

The loading setup for specimen SP-3 was similar to that of specimen SP-2. Two types of loading were applied. Firstly, the maximum load was limited to service load, while the load was increased to the ultimate state in the second type. In load setup SP-3-L01, the maximum load was limited to the service load. Maximum positive and negative strains recorded were lower than the yield strain with corresponding values of 1470 and 800 microns, respectively, as shown in Figure 20a, whereas for the load setup SP-3-L02, the load was increased to the ultimate load. As seen in Figure 20b, the maximum positive strain was around 2500 microns, which is higher than the yield strain of steel bars. However, a similar value of negative strain was not observed as the maximum value was limited to only 1200 microns.

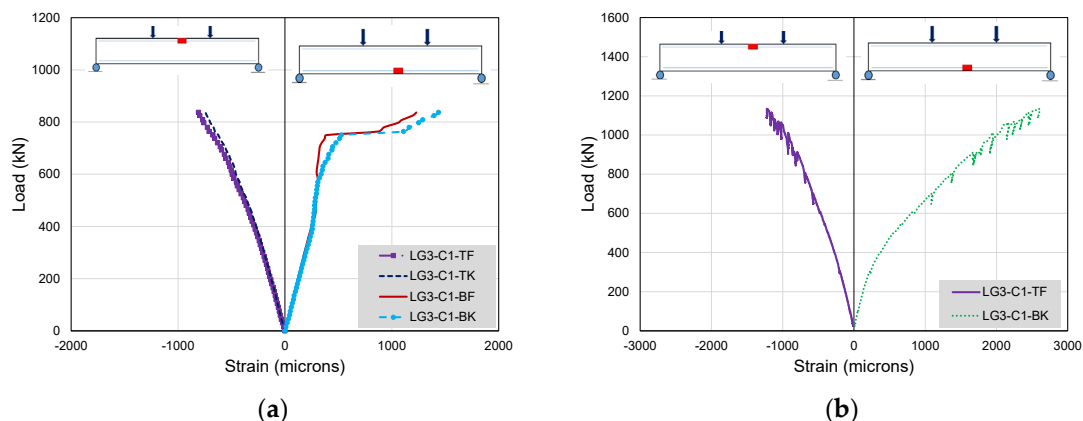


Figure 20. Strain versus load responses (a) load setup SP-3-L01 and (b) load setup SP-3-L02.

7.2. Comparison of Longitudinal Steel Strains

This section presents a comparison of steel strains recorded among three specimens. Specimen SP-1 was subjected to four types of loadings (i.e., SP-1-L01, SP-1-L02, SP-1-L03, and SP-1-L04). Specimen SP-2 was flexure-dominated, subjected to two types of

loadings, i.e., SP-2-L01 and SP-2-L02. Similarly, specimen SP-3 was shear dominated and was subjected to loadings SP-3-L01 and SP-3-L02. The comparison is made on the basis of the similarity between the loading type and span characteristics. For instance, loading SP-2-L01 refers to a two-point service load applied to specimen SP-2, which was designed to dominate in flexure. Corresponding strain components in a three-span specimen are found under the loading type SP-1-L02, i.e., two-point service load applied to the interior span of specimen SP-1.

7.2.1. Comparison under Two-Point Service Loads

Comparison between SP-1-L02 and SP-2-L01

Loading types SP-1-L02 and SP-2-L01 refer to the application of two-point service load to the interior span of specimen SP-1 and specimen SP-2, respectively. The comparison is made possible since both the interior span of specimen SP-1 and specimen SP-2 were supposed to dominate in flexure. Maximum positive and negative strains recorded for loading setup SP-2-L01 were 320 and 210 microns, respectively (see Figure 21a). It is evident that under service loads, maximum positive strains recorded in the interior span of continuous girder were lower than those recorded on longitudinal steel bars of a single-span girder (see strains for SP-1, for instance). A similar trend was observed for negative strains as well, as presented in Figure 21b.

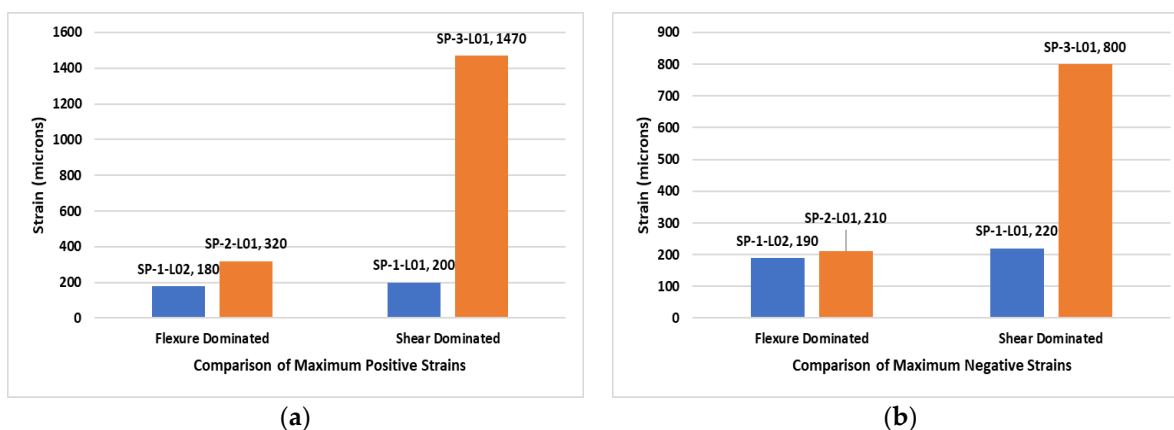


Figure 21. Comparison of strain under two-point service load (a) positive and (b) negative strain.

Comparison between SP-1-L01 and SP-3-L01

Specimen SP-3 was designed to dominate in shear. Therefore, its comparison was made with the response of exterior girders of specimen SP-1. Under two-point service load conditions, corresponding loading setups for specimen SP-1 and SP-3 were SP-1-L01 and SP-3-L01, respectively. Analogous to the flexure-dominated specimen, maximum positive and negative strains recorded in shear-dominated specimen SP-3 were significantly higher than their counterpart strain values recorded in specimen SP-1. The results are presented in Figure 21a,b for positive and negative strains, respectively.

7.2.2. Comparison under Four-Point Service Loads for SP-1 and Two-Point Service Loads for SP-2 and SP-3

Specimen SP-1 was subjected to a four-point service load at its interior and left exterior spans. Strains monitored at the interior span are compared with those monitored in specimen SP-2 under service loads. Similarly, strains monitored at the exterior span of specimen SP-1 are compared with those monitored in specimen SP-3 under service loads.

Comparison between SP-1-L03 and SP-2-L01

The transition from two-point to four-point loading did not significantly change the trend, as was observed for the loading SP-1-L01 and SP-1-L02. Strains monitored at

the interior span of specimen SP-1 were noticeably lower than their counterpart values measured in specimen SP-2 under service loads. This trend was held for both positive and negative strains, as shown in Figure 22a,b.

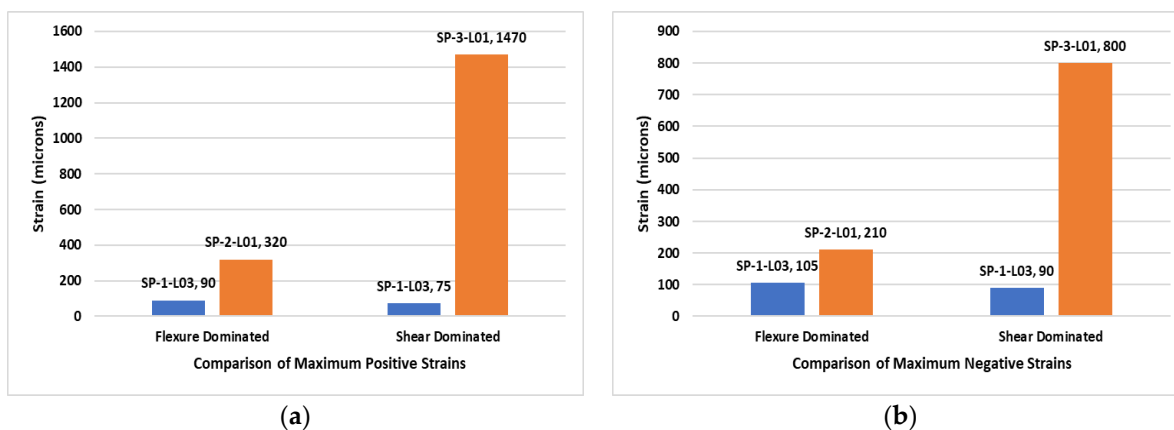


Figure 22. Comparison of strain under four-point service load (a) positive and (b) negative strain.

Comparison between SP-1-L03 and SP-3-L01

This section compares maximum longitudinal steel strains recorded at the exterior span of specimen SP-1 with those measured in specimen SP-3 under service loads. Maximum positive and negative strains recorded in specimen SP-1 under load type SP-1-L03 were 105 and 90 microns, respectively. On the contrary, the maximum positive and negative strains in specimen SP-3 were 1470 and 800 microns, respectively.

7.2.3. Comparison under Four-Point Ultimate Loads for SP-1 and Two-Point Ultimate Loads for SP-2 and SP-3

Comparison under this category is made in a similar manner as the previous section. The concerned loading setups for specimens SP-1, SP-2, and SP-3 in this category are SP-1-L04, SP-2-L02, and SP-3-L03, respectively.

Comparison between SP-1-L04 and SP-2-L02

Load setup SP-1-L04 corresponds to a four-point ultimate load applied to the interior and left exterior spans of specimen SP-1, while load setup SP-2-L02 represents a two-point ultimate load applied to specimen SP-2. As shown in Figure 23a,b, maximum positive and negative strains for SP-1-L04 were 500 and 750 microns, respectively. On the other hand, maximum positive and negative strains for SP-2-L02 were 3000 and 2000 microns, respectively. This agrees with previous load cases, as longitudinal steel strains recorded in continuous girder SP-1 were found to be significantly lower than those recorded in specimen SP-2 under similar load conditions.

Comparison between SP-1-L04 and SP-3-L02

A similar trend to that of flexure-dominated specimens was also observed in the shear-dominated specimen. Load setup SP-3-L02 corresponds to a two-point ultimate load subjected to specimen SP-2, which was designed to dominate in shear. However, results from Figure 23a,b confirm that longitudinal steel strains are significantly overestimated in single-span girders, which incorporated similar structural details to those of the exterior girders of specimen SP-1. Despite having similar structural details and loading conditions, strains recorded in the single-span shear-dominated specimen (i.e., specimen SP-3) reached almost double the values of those recorded in specimen SP-1.

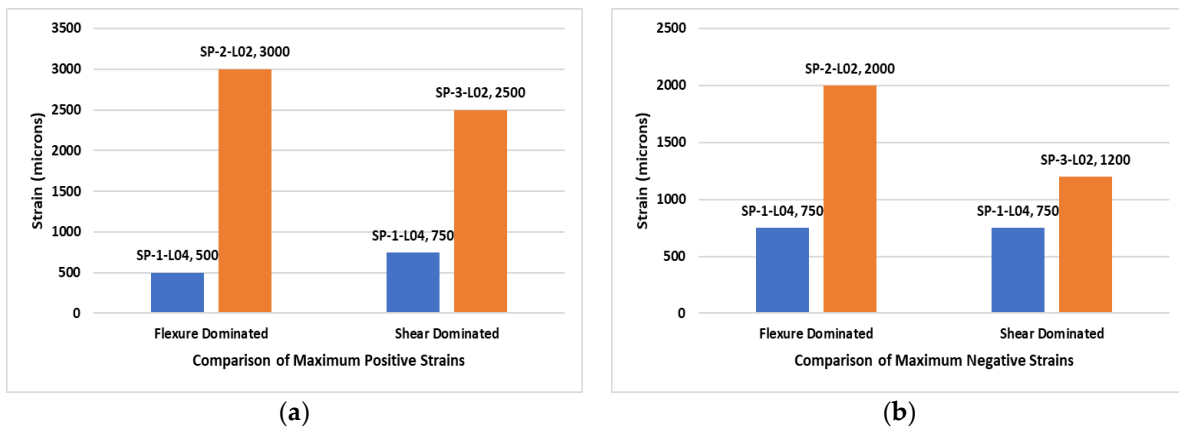


Figure 23. Comparison of strain under four-point service load (a) positive and (b) negative strain.

7.3. Transverse Reinforcement Strains

Strain gages were also mounted on stirrups of each specimen near their supports. At each support, the strain was measured on three different stirrups.

7.3.1. Specimen SP-1

Loading Setup SP-1-L01

This loading setup corresponds to the application of a two-point service load at the right exterior span of specimen SP-1. Figure 24a shows the stirrup strain distribution versus applied load for D4–D6. It can be seen that the maximum strain recorded was below 100 microns, which is significantly lower than the yield strain of stirrups. Recorded strains at locations E10–E12 are presented in Figure 24b. Maximum strains recorded here were noticeably lower than those recorded at D4–D6, with maximum value limited to 17 microns.

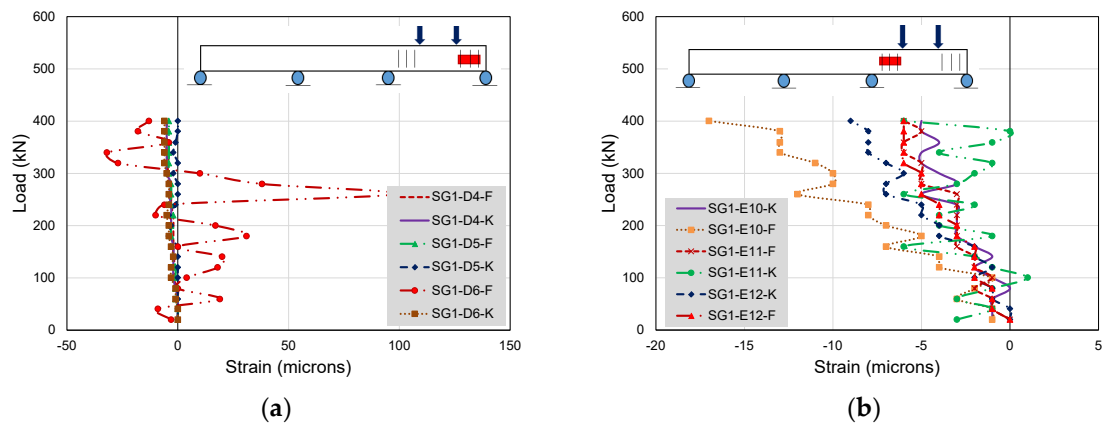


Figure 24. Load versus strain responses in load setup SP-1-L01 (a) D4–D6 and (b) E10–E12.

Loading Setup SP-1-L02

This load setup corresponds to the application of a two-point service load at the interior span of specimen SP-1. The concerned stirrup strain gages under this setup were E4–E6 (at the interior face of left interior support) and E7–E9 (at the interior face of right interior support). Figure 25a shows the monitored strains for E7–E9 gages. Maximum strains were below 7 microns. Similarly, Figure 25b presents strains recorded at the E4–E6 gages. It can be seen that the maximum strains recorded at this location were slightly higher than 10 microns. A very small strain around 10 microns suggested that this span was not shear critical.

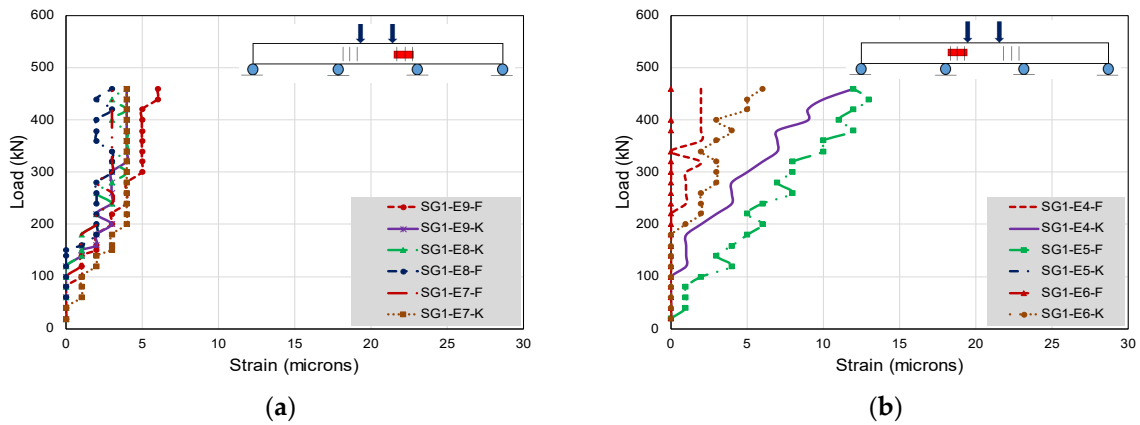


Figure 25. Load versus strain responses in load setup SP-1-L02 (a) E7–E9 and (b) E4–E6.

Loading Setup SP-1-L03

Under this loading setup, four-point loading was applied to interior and left exterior spans up to the service limit. The recorded strain data are plotted in Figure 26. Due to the damage to strain gages D2, D3, E1, and E3, only data for strain gages D1 and E3 are plotted in Figure 26a,b, respectively. Maximum strains recorded at D1–D3, E1–E3, E4–E6, and E7–E9 were limited to 590, 5, 15, and 7 microns, respectively. It is evident that the exterior span was shear critical, as negligible stirrup strains were recorded within the interior span under a four-point service load.

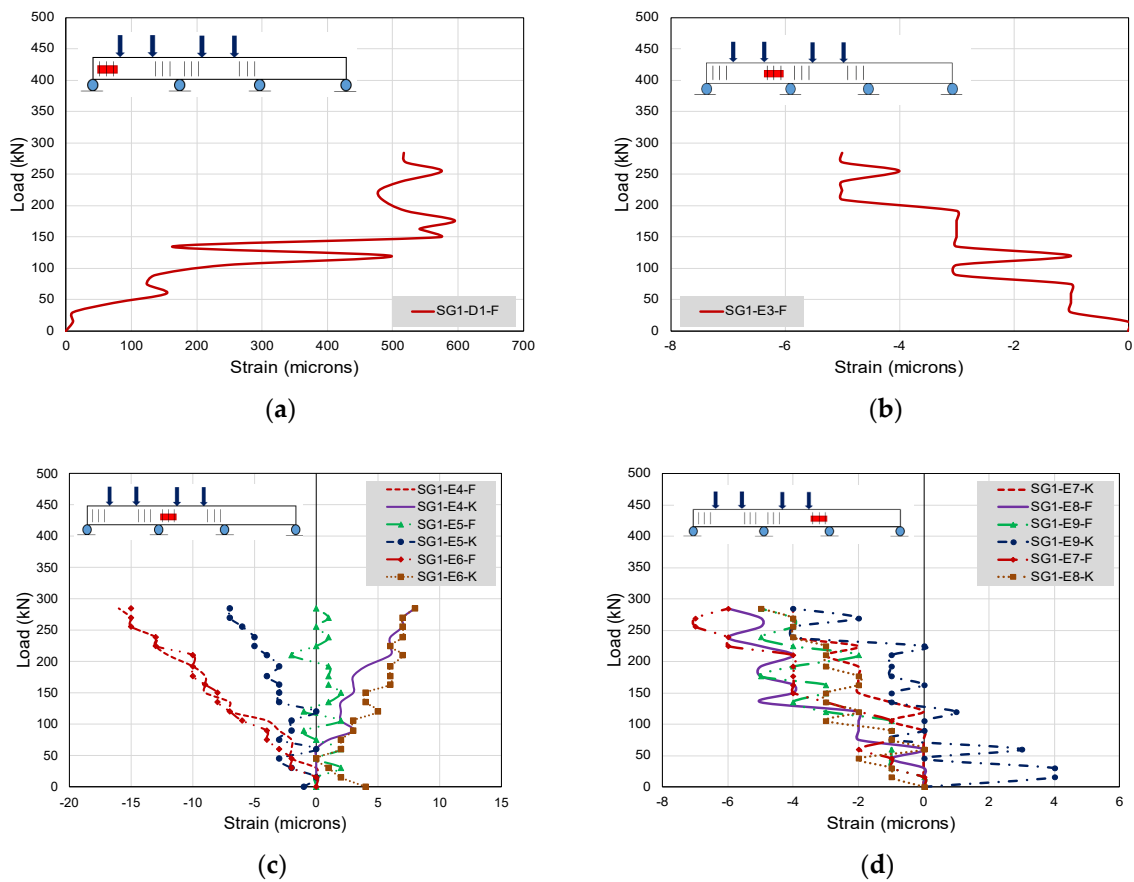


Figure 26. Load versus strain responses in load setup SP-1-L03 (a) D1, (b) E3, (c) E4–E6, and (d) E7–E9.

Loading Setup SP-1-L04

This loading was similar to SP-1-L03 but with an increased intensity of load to the ultimate state. Concerned stirrup locations were again E1–E3 (at the exterior face of left interior support), E4–E6, and E7–E9. The corresponding strain data are plotted in Figure 27. It is to be mentioned that unreliable data were obtained at the D1–D3 location. Therefore, these data are not presented here for clarity. Some strain gauges were also damaged at the remaining locations. Therefore, only available strain gauge data are plotted for locations E1–E3, E4–E6, and E7–E9, respectively. With reference to these locations, maximum strains were limited to 110, 400, and 15 microns for E1–E3, E4–E6, and E7–E9, respectively. Recorded strains were significantly lower than the yield strain of stirrups under ultimate load.

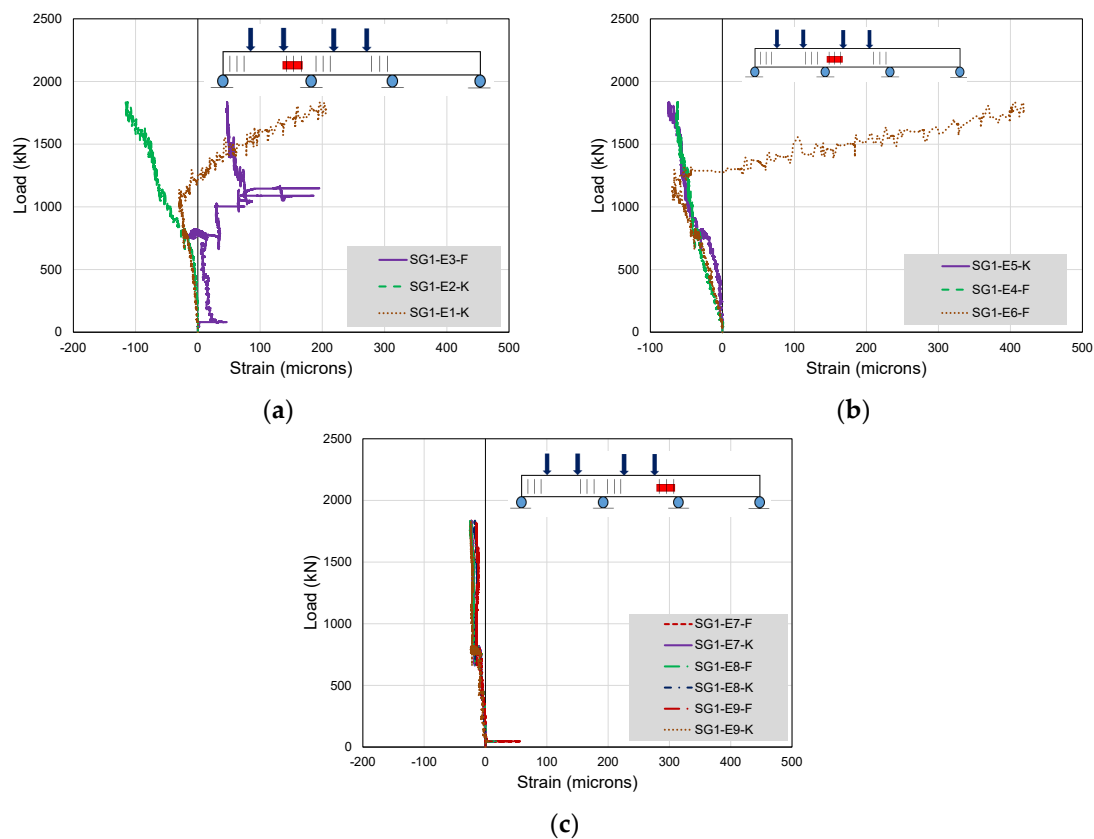


Figure 27. Load versus strain responses in load setup SP-1-L04 (a) DE1-E3, (b) E4-E6, (c) E7-E9.

7.3.2. Specimen SP-2

As mentioned in earlier sections, specimen SP-2 was a single-span girder subjected to two-point service and ultimate loads. Further, this specimen was designed to dominate in flexure and replicate the design details of the interior span of specimen SP-1. Similar to specimen SP-1, strain gauges were also attached to the stirrups of specimen SP-2. Six strain gauges were attached to stirrups at each end of specimen SP-2. These six strain gauges were distributed to three stirrups with two gages at each stirrup. Their location is designated by D1–D3 and D4–D6 for left and right end stirrups, respectively. In loading setup SP-2-L01, a two-point load was applied with a magnitude limited to the service load capacity. Recorded strains at D1–D3 and D4–D6 are plotted in Figure 28a,b, respectively. Maximum stirrup strains recorded under the service load were limited to 6 and 15 microns on the left and right sides, respectively. These low strains indicate that shear demand on specimen SP-2 under service loads was negligible. In loading setup SP-2-L02, the specimen SP-2 was subjected to a two-point ultimate load. Concerned strain locations were similar to those of the loading setup SP-2-L01. The plot in Figure 29a,b measured strains at locations D1–D3 and D4–D6, respectively. Corresponding maximum values of strains were limited to 41 and

70 microns, respectively. Some strain gauges, such as SG2-D1-F and SG2-D5-K, showed negative values. However, the small values of strain suggest that specimen SP-2 did not experience significant shear demand even under ultimate loads.

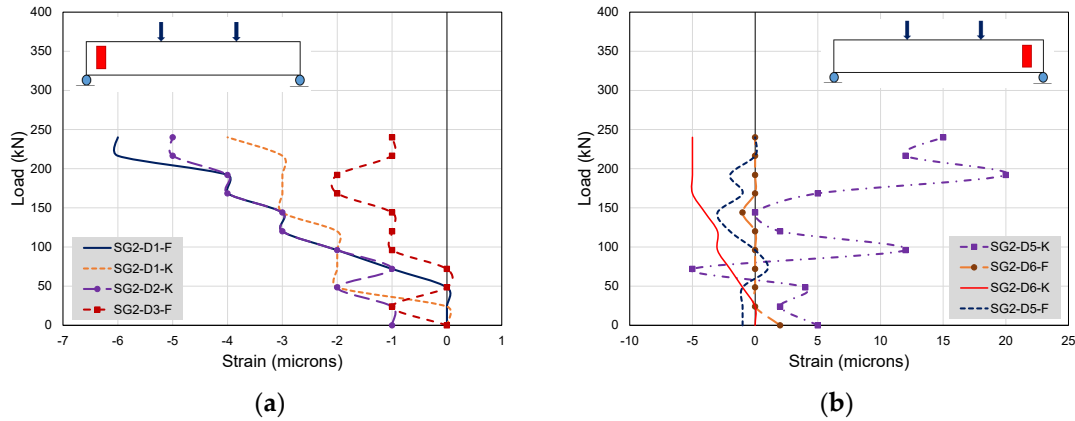


Figure 28. Load versus strain responses in load setup SP-2-L01 (a) D1–D3, and (b) D5–D6.

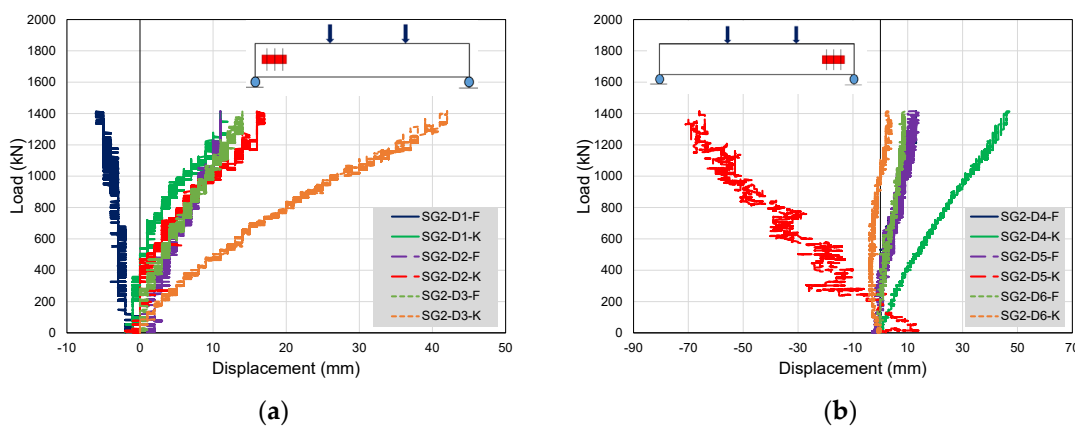


Figure 29. Load versus strain responses in load setup SP-2-L02 (a) D1–D3, and (b) D5–D6.

7.3.3. Specimen SP-3

Specimen SP-3 was again a single-span girder subjected to two-point service and ultimate loads. However, it was designed to experience higher shear demands in comparison to specimen SP-2 to be compared with exterior spans of specimen SP-1. A similar nomenclature to those of specimen SP-2 was adopted for specimen SP-3 for ease of comparison. In loading setup SP-3-L01, the maximum strains recorded at positions D1–D3 and D4–D6 were limited to 20 and 17 microns, respectively, as shown in Figure 30a,b. These values are significantly lower than the yield strain of stirrups. In loading setup SP-3-L02, specimen SP-3 experienced very low strains, as maximum strains at positions D1–D3 and D4–D6 were limited to 13 and 20 microns, respectively (see Figure 31a,b). This suggests that SP-3 did not experience considerable shear demand.

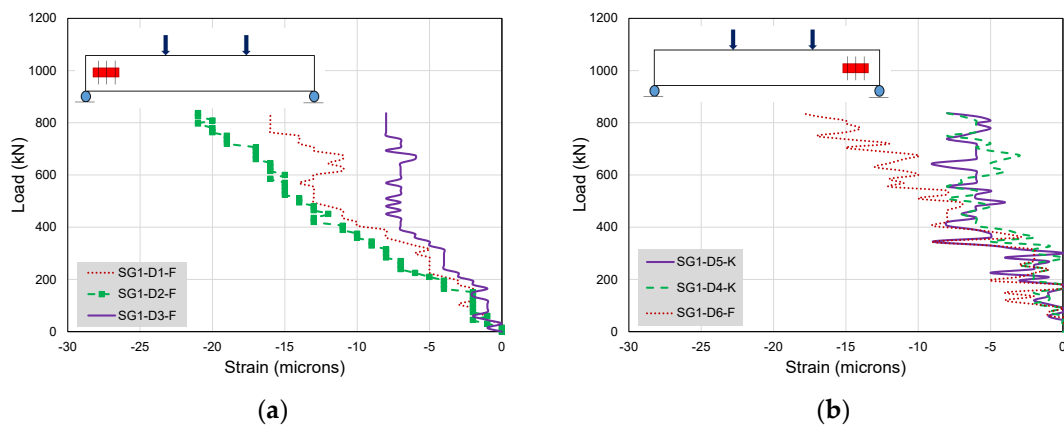


Figure 30. Load versus strain responses in load setup SP-3-L01 (a) D1–D3, and (b) D4–D6.

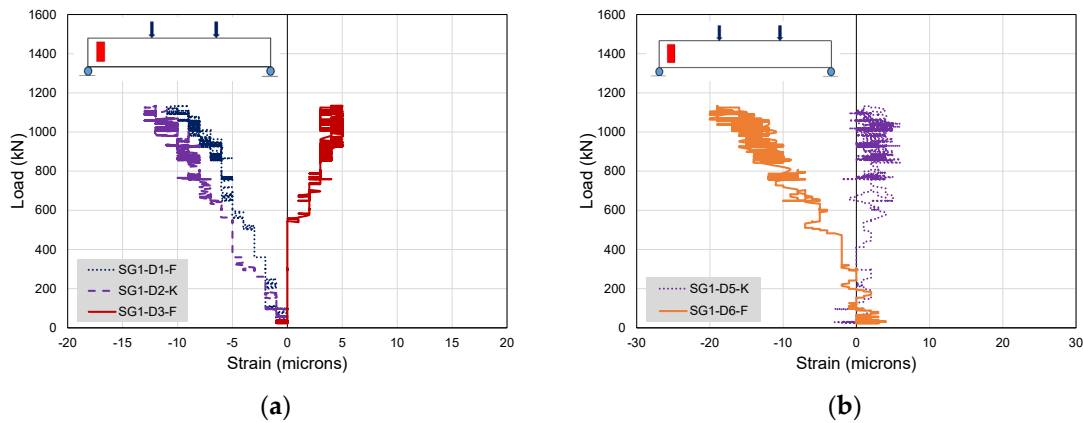


Figure 31. Load versus strain responses in load setup SP-3-L02 (a) D1–D3 and (b) D4–D6.

7.4. Comparison of Stirrup Strain

This section presents a comparison of maximum stirrup strains monitored among three specimens. The comparison is made on the basis of the resemblance between the loading type and span's attributes. For instance, loading SP-2-L01 refers to a two-point service load applied to specimen SP-2, which was designed to dominate in flexure. Corresponding strain components in a three-span specimen are found under the loading type SP-1-L02, i.e., two-point service load applied to the interior span of specimen SP-1.

7.4.1. Comparison under Two-Point Service Load

Comparison between SP-1-L02 and SP-2-L01

Loading setup SP-1-L02 and SP-2-L01 correspond to the application of a two-point service load on the interior span of specimens SP-1 and SP-2, respectively. The comparison is plotted in Figure 32. It is evident that maximum strains recorded among these loading setups were comparable and remained below 15 microns. Both these spans were intended to dominate in flexure. This was demonstrated by their low shear strains recorded experimentally.

Comparison between SP-1-L01 and SP-3-L01

Loading setups SP-1-L01 and SP-3-L01 represented the application of a two-point service load on the right exterior span of specimen SP-1 and specimen SP-3. Both these spans were designed to dominate in shear. At the exterior face of the left interior support of specimen SP-1, the maximum shear strain was comparable to that recorded at the corresponding position in specimen SP-3, i.e., at position D1–D3. However, the maximum

shear strain at position D4–D6 in specimen SP-1 was approximately six-times higher than that recorded at the corresponding position in specimen SP-3, as shown in Figure 33.

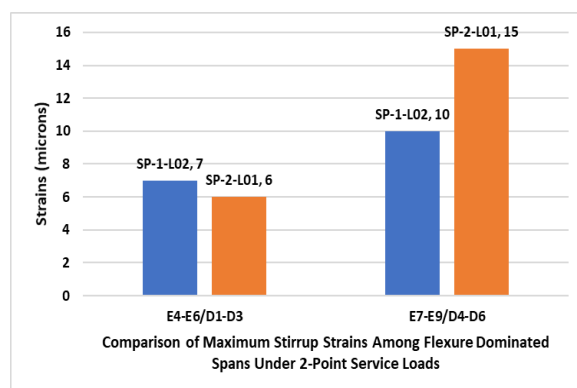


Figure 32. Comparison of maximum stirrup strains recorded for loading setup SP-1-L02 and SP-2-L01 under two-point service loads.

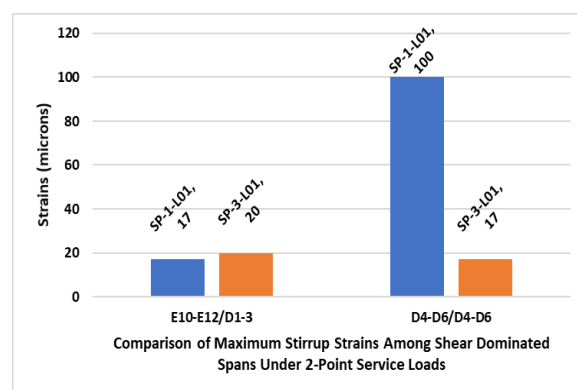


Figure 33. Comparison of maximum stirrup strains recorded for loading setup SP-1-L01 and SP-3-L01 under two-point service loads.

7.4.2. Comparison under Four-Point Service Load

Loading setups SP-1-L03, SP-2-L01, and SP-3-L01 fit into this category.

Comparison between SP-1-L03 and SP-2-L01

Loading setup SP-1-L03 corresponds to the application of a four-point service load on specimen SP-1. Its comparison with SP-2-L01 is plotted in Figure 34. Neither of the two load cases induced considerable strains in stirrups. This was expected, as both the load cases described in this section belonged to flexure-dominated spans.

Comparison between SP-1-L03 and SP-3-L01

This section is similar to the previous section, except that the load case SP-1-L03 is compared with SP-3-L01. Since SP-3-L01 corresponds to the shear-dominated single-span girder subjected to service loads, its maximum stirrup strains are compared with those measured at the left-exterior span of specimen SP-1. A comparison of maximum stirrup strains in this category is presented in Figure 35. At the left exterior span of specimen SP-1, stirrup strains reached approximately 590 microns. On the contrary, specimen SP-3 did not mobilize strains of the same magnitude at its corresponding location.

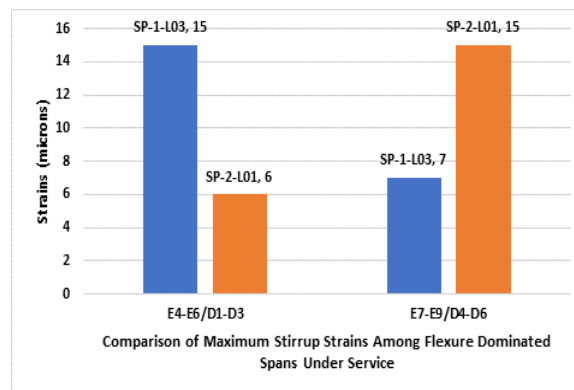


Figure 34. Comparison of maximum stirrup strains recorded for loading setup SP-1-L03 and SP-2-L01 under four-point service loads.

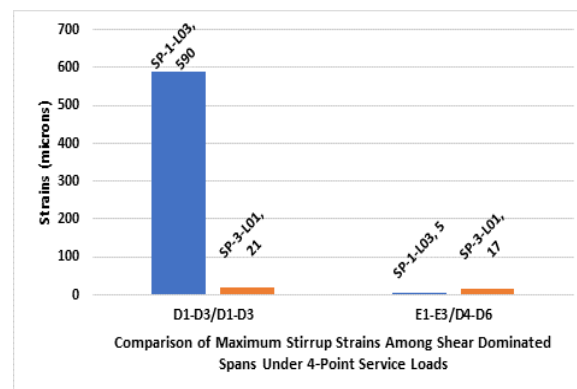


Figure 35. Comparison of maximum stirrup strains recorded for loading setup SP-1-L03 and SP-3-L01 under four-point service loads.

7.4.3. Comparison under Four-Point Ultimate Load

Load cases SP-1-L04, SP-2-L02, and SP-3-L02 fall in this category.

Comparison between SP-1-L04 and SP-2-L02

These cases correspond to the application of four-point and two-point ultimate loads on specimens SP-1 and SP-2, respectively. Since specimen SP-2 was a flexure-dominated girder, its comparison was made with the interior span of specimen SP-1, which was supposed to dominate in flexure as well. The comparison of maximum stirrup strains is presented in Figure 36. It can be seen that stirrup strains reached approximately 400 microns at the interior face of the left interior support of specimen SP-1. However, stirrup strains at the corresponding location in specimen SP-2 could not achieve a similar magnitude.

Comparison between SP-1-L04 and SP-3-L02

In this category, stirrup strains recorded at the left exterior span of specimen SP-1 are compared with those recorded in the stirrups of specimen SP-3 subjected to ultimate loads. The comparison is presented in Figure 37. This comparison is, again, consistent with previous results. Specimen SP-1, which was a three-span girder, was able to mobilize higher strains in stirrups at the exterior face of left interior support than the corresponding strains recorded in specimen SP3. It is worth mentioning that both load cases were designed to dominate in shear. However, single-span specimen SP3 exhibited lower demand on stirrups than that imposed by specimen SP-1. Due to the malfunction of strain gages at the left exterior support of specimen SP-1, no reliable data could be obtained.

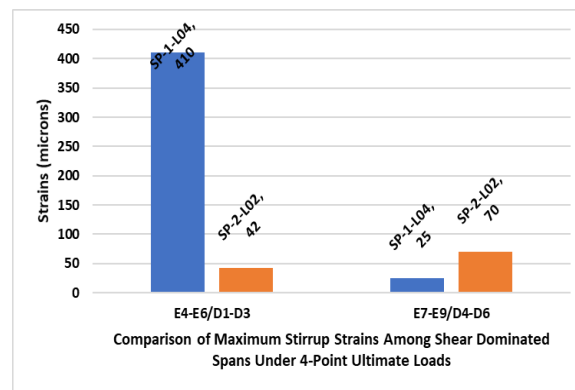


Figure 36. Comparison of maximum stirrup strains recorded for loading setup SP-1-L04 and SP-2-L02 under four-point ultimate loads.

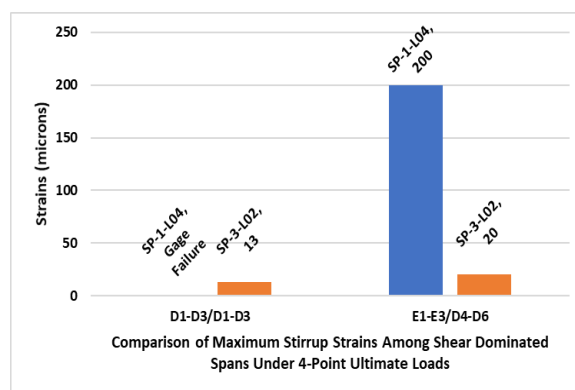


Figure 37. Comparison of maximum stirrup strains recorded for loading setup SP-1-L04 and SP-3-L02 under four-point ultimate loads.

7.5. Tendon Strains

Some strain gauges were mounted on tendons to monitor their strains during each loading application (see Section 5). Further results are discussed in the following sections.

7.5.1. Tendon Strains in Specimen SP-1

Loading Setup SP-1-L01

Figure 38a,b present recorded tendon strains at locations C3 and A3, respectively. Maximum recorded strains at these locations were 175 and 117 microns, respectively. It is to be mentioned that a number of strain gauges on tendons failed and only reliable results are presented. Further, these strains remained well below the yield strains of tendons, indicating no permanent damage to tendons under two-point service loads on the right exterior girder.

Loading Setup SP-1-L02

Under the application of two-point service load on the interior span of specimen SP-1, recorded strains on tendons are presented in Figure 39a,b for locations A2 and C2, respectively. Since the loads were limited to the service load magnitude, which is implicitly contained within the yield limits of the longitudinal steel bars, maximum tendon strains remained well below their yield limits with their magnitudes 125 and 170 microns at locations A2 and C2, respectively.

Loading Setup SP-1-L03

Figure 40 presents recorded tendon strains during the application of a four-point service load on specimen SP-1. It can be seen that strains remain linear at the C1, A2, C2, and A3 locations, with maximum recorded strains as 81, 125, 170, and 50 microns, respectively. This suggests that none of the tendons yielded during the application of four-point service loads.

Loading Setup SP-1-L04

This loading setup corresponds to the application of four-point ultimate loading on specimen SP-1. It can be seen from Figure 41 that tendons did not yield at locations C1, C2, and A3. Tendon strains more than their yield strains were only recorded at the left interior support, with a magnitude of approximately 4000 microns.

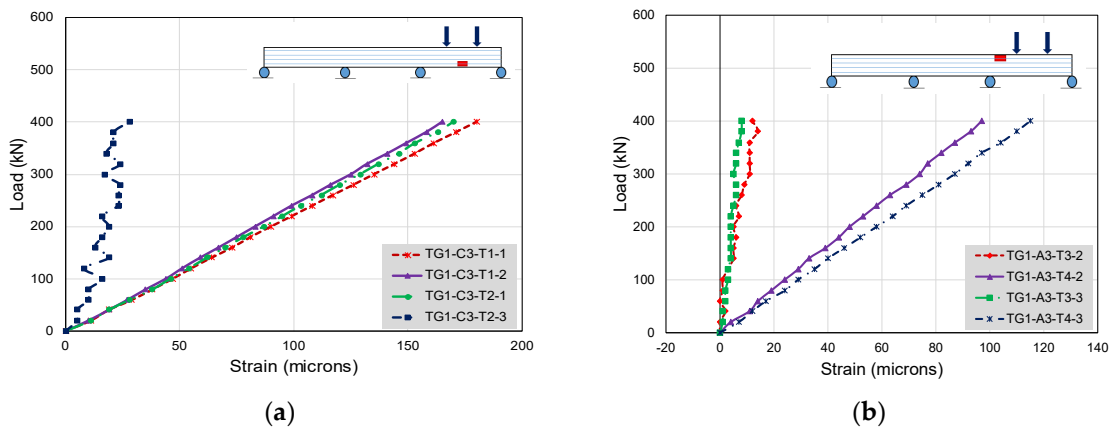


Figure 38. Load versus strain responses in load setup SP-1-L01 (a) C3 and (b) A3.

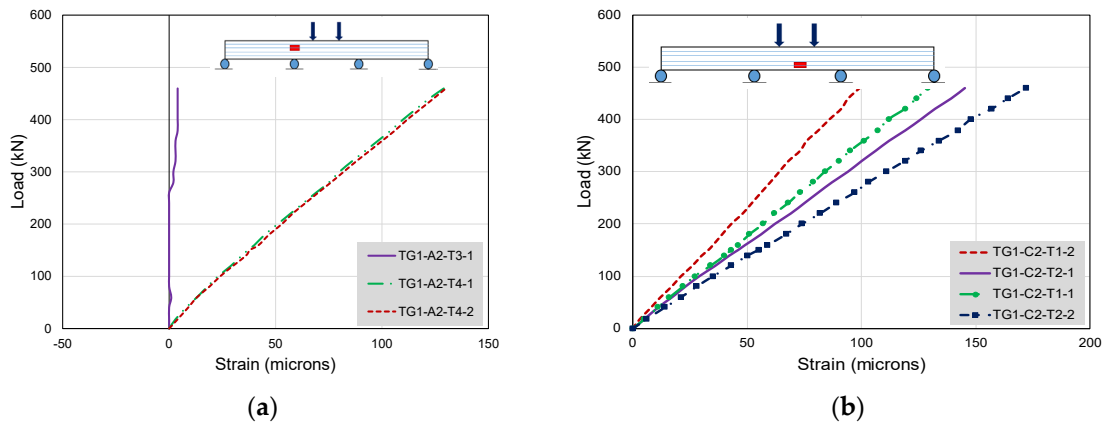


Figure 39. Load versus strain responses in load setup SP-1-L02 (a) A2 and (b) C2.

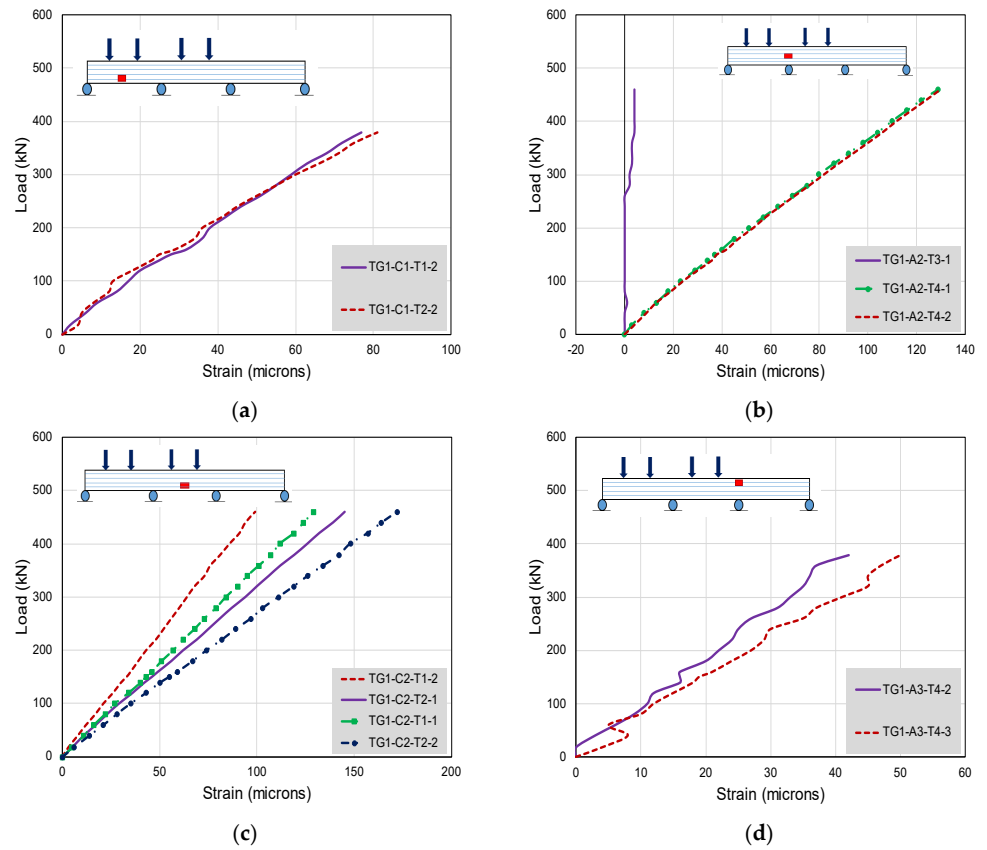


Figure 40. Tendon strains recorded during loading setup SP-1-L03 at locations (a) C1, (b) A2, (c) C2, and (d) A3.

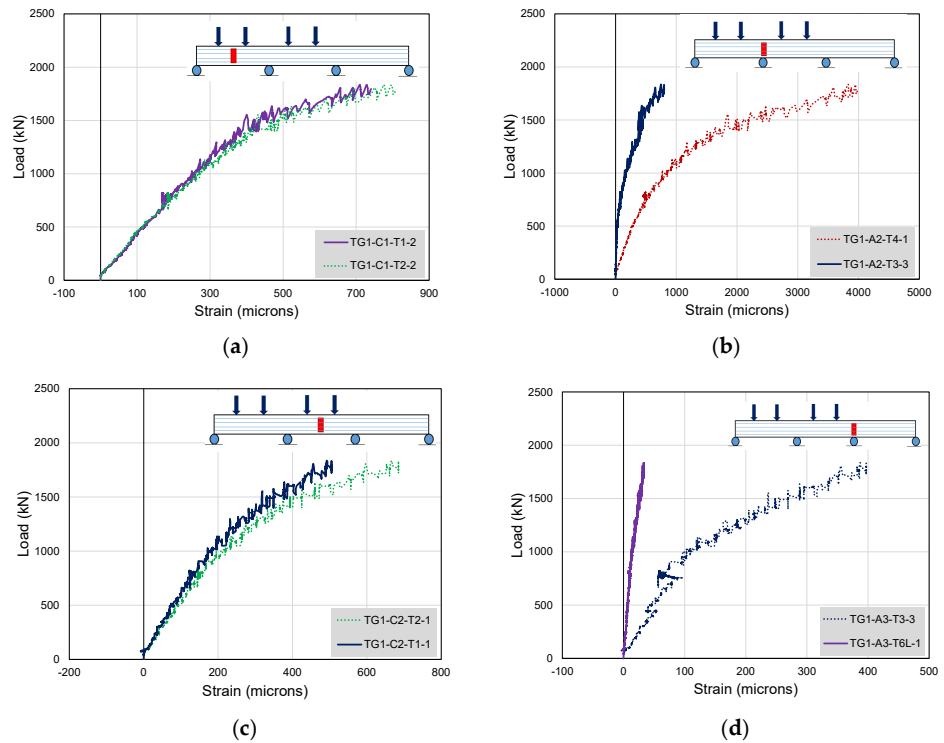


Figure 41. Tendon strains recorded during loading setup SP-1-L04 at locations (a) C1, (b) A2, (c) C2, and (d) A3.

7.5.2. Tendon Strains in Specimen SP-2

Figure 42a presents recorded tendon strains at the midspan (i.e., location C1) of specimen SP-2 under two-point service loads, i.e., SP-2-L01. Strains were limited to 80 microns and well below the yield strain of tendons. In loading setup SP-2-L02, tendon strains as high as 475 microns were reported before the failure of strain gauges, as shown in Figure 42b.

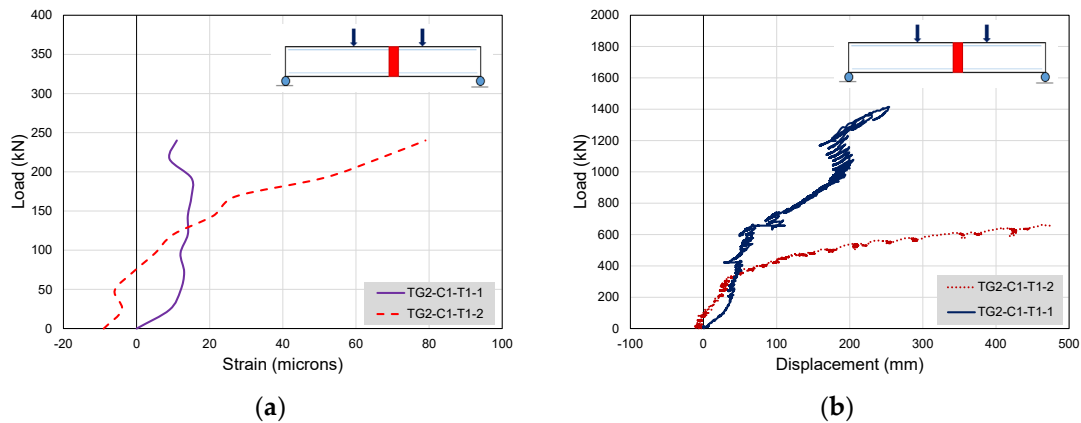


Figure 42. Load versus strain responses at location C1 (a) load SP-2-L01 (b) load SP-2-L02.

7.5.3. Tendon Strains in Specimen SP-3

In loading setup SP-3-L01, recorded strains on specimen SP-3 correspond to the location C1, i.e., at its midspan. Figure 43a shows recorded tendon strains during loading setup SP-3-L01. It can be seen that strains did not enter the yield plateau and were limited to 890 microns, whereas in loading setup SP-3-L02, maximum tendon strain was limited to 1750 microns (see Figure 43b). Unlike specimen SP-2, which was expected to dominate in flexure, specimen SP-3 did not mobilize tendon strains beyond their yield strains.

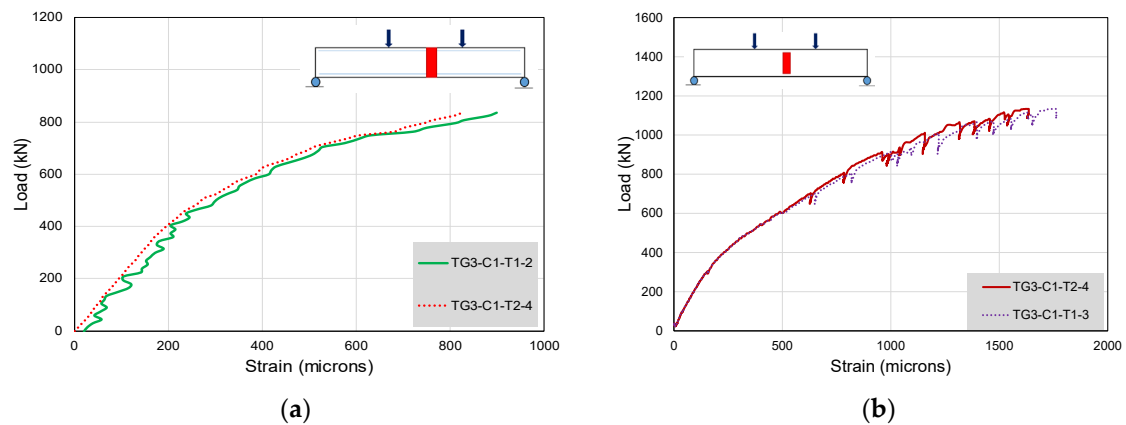


Figure 43. Load versus strain responses at location C1 (a) load SP-3-L01 (b) load SP-3-L02.

7.6. Comparison of Tendon Strains

In this section, maximum tendon strains recorded are compared among specimens SP-1, SP-2, and S-3. Comparison criteria are kept the same as for previous sections.

7.6.1. Comparison of Tendon Strains under Two-Point Service Loads

Comparison between Loading Setup SP-1-L01 and SP-3-L01

This section compares the maximum tendon strains obtained in specimens SP-1 and SP-3 under two-point loading. The comparison is made only at midspans due to the limitation on the availability of tendon strains in specimen SP-3. A comparison is shown in Figure 44 and it can be seen that the maximum tendon strain recorded in specimen SP-3

was approximately four-times higher than the corresponding tendon strain in specimen SP-1 under service loads. Nonetheless, maximum strains in both cases remained well below the yield strains of tendons.

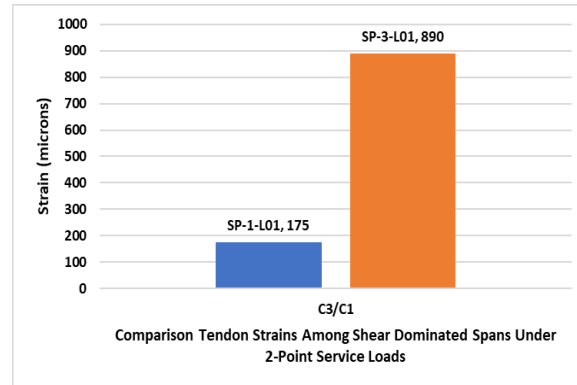


Figure 44. Comparison of maximum tendon strains recorded under two-point service loads between specimen SP-1 and SP-3.

Comparison between Loading Setup SP-1-L01 and SP-2-L01

This section compares maximum tendon strains recorded in specimens SP-1 and SP-2 under two-point service loads. As shown in Figure 45, both strain values were comparable and maximum strains were limited well below the yield strain limits of tendons.

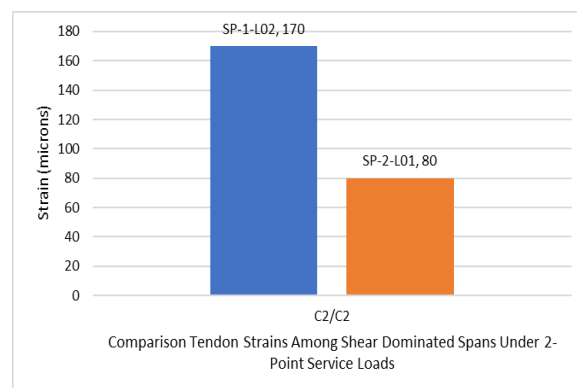


Figure 45. Comparison of maximum tendon strains recorded under two-point service loads between specimen SP-1 and SP-2.

7.6.2. Comparison of Tendon Strains under Four-Point Service Loads

Comparison between Loading Setup SP-1-L03 and SP-3-L01

Loading setup SP-1-L03 corresponds to the application of a four-point service load on specimen SP-1. Maximum tendon strain recorded at the exterior span is compared with that recorded in specimen SP-3 under service loads, as shown in Figure 46. The trend is similar to that obtained under two-point service loads, with tendon strain in specimen SP-3 reaching as high as 890 microns, whereas the corresponding tendon strain in SP-1 only reached 80 microns.

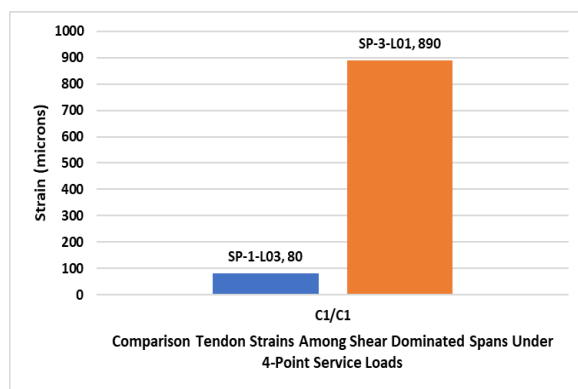


Figure 46. Comparison of maximum tendon strains recorded under four-point service loads between specimen SP-1 and SP-3.

Comparison between Loading Setup SP-1-L03 and SP-2-L01

Loading setup SP-1-L03 corresponds to a four-point service load on specimen SP-1. Under this load, maximum tendon strain recorded at the midspan of the interior girder is compared with that recorded in specimen SP-2, as shown in Figure 47. Analogous to the comparison between the same specimens under two-point loading, maximum strains recorded in two specimens under four-point loading were comparable.

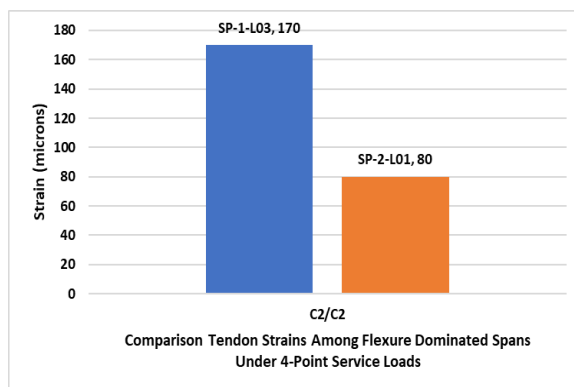


Figure 47. Comparison of maximum tendon strains recorded under four-point service loads between specimen SP-1 and SP-2.

7.6.3. Comparison of Tendon Strains under Four-Point Ultimate Loads

Comparison between Loading Setup SP-1-L04 and SP-3-L02

Figure 48 shows that under the ultimate loads, specimen SP-3 was able to mobilize tendon strains up to 1750 microns, which were twice as high as the tendon strains recorded in specimen SP-1. However, both the specimens were not able to achieve the yield state in tendons even under ultimate loads.

Comparison between Loading Setup SP-1-L04 and SP-2-L02

The maximum tendon strains are compared between specimen SP-1 and SP-2 in this section, with the exception that the load magnitude was increased to the ultimate limit. Figure 49 presents the maximum recorded tendon strains in this category. Specimen SP-1 was able to record tendon strains in excess of the yield limit. However, single-span specimen SP-2 was able to record 10-times lesser strains than those mobilized by specimen SP-1 under ultimate loads, which is basically due to the damage to the strain gauge.

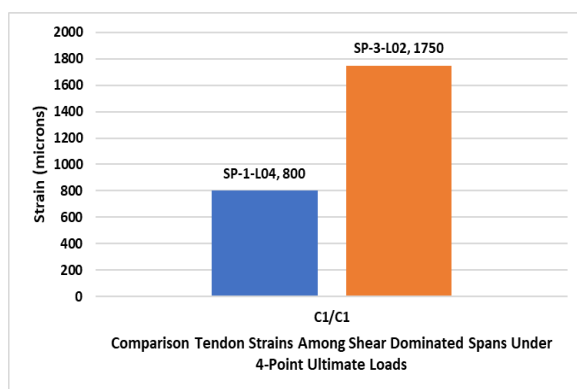


Figure 48. Comparison of maximum tendon strains recorded under four-point ultimate loads between specimen SP-1 and SP-3.

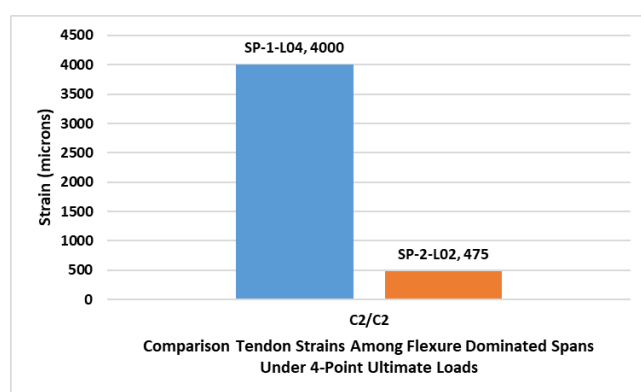


Figure 49. Comparison of maximum tendon strains recorded under four-point ultimate loads between specimen SP-1 and SP-2.

7.7. Ultimate Deflections and Failure Modes

The comparison of the load–deflection curves of specimen SP-2 and the interior span of specimen SP-1 under ultimate load is summarized in Table 4. It is obvious that the single-span flexure-dominated girder could not replicate the structural behavior of its counterpart girder in the continuous girder system. The interior girder of specimen SP-1 was able to sustain a higher load as compared to specimen SP-2, whereas the maximum deflection sustained by specimen SP-2 was higher than that of the interior span of specimen SP-1.

Table 4. Comparison of the ultimate load and deflection for specimen SP-1 and SP-2.

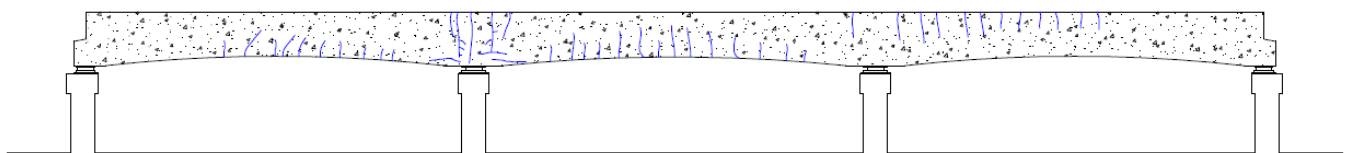
Specimen	Ultimate Load (kN)	Ultimate Deflection (mm)
SP-1 (interior girder)	2740	212
SP-2	1405	297

The ultimate deflection of the exterior girder of specimen SP-1 was not recorded during the test. Therefore, the comparison of specimen SP-3 and the exterior span of specimen SP-1 two-point and four-point service loads is summarized in Table 5. For specimen SP-1 under two-point and four-point loads, the maximum deflection was lower than the corresponding deflection in specimen SP-3. Unlike the case of specimen SP-2, the maximum sustained load for specimen SP-3 was higher than specimen SP-1.

Table 5. Comparison of the load–deflection values for exterior girder of specimen SP-1 and specimen SP-3 under service loads.

Specimen	Peak Service Load (kN)	Peak Service Deflection (mm)
SP-1 (two-point load)	400	22
SP-1 (four-point load)	300	9
SP-3	800	96

Further, under the service loads, no cracks were observed in specimen SP-1 at any location. The first cracks were observed in the midspan of the interior girder at a load of 550 kN. Cracks started to appear in negative moment regions near wet joints at a load of 800 kN. The first flexural crack in the midspan of the left exterior girder was observed at a load of approximately 1200 kN. No flexural cracks were observed in the right exterior girder till a load of 2000 kN. At this stage, the first crack appeared in the negative moment region of the right exterior girder. At the ultimate load, wide flexural cracks were observed, whereas severe cracking was observed near the wet joints. In addition, severe crushing of concrete was observed near the supports (Figure 50).



(a)



(b)

Figure 50. Ultimate failure of specimen SP-1, (a) line diagram, (b) concrete crushing.

Specimen SP-2 did not exhibit any cracking under the service loads. Cracks in the positive and negative moment region of the left support started to appear at the load of 475 kN. Cracks near the right support appeared at the load of approximately 575 kN. A further increase in the load witnessed widening and propagation of cracks along the height of the girder. The final failure of specimen SP-2 accompanied severe concrete crushing and bearing support failure (Figure 51). Similar to specimens SP-1 and SP-2, no cracks were observed in specimen SP-3 within the service load limits. The first flexural cracks were observed at the load of 510 kN, whereas the first cracks at the right and left supports were observed at loads of 600 and 700 kN, respectively. The final failure of

specimen SP-3 also experienced concrete crushing in the compression zone of midspan, buckling of longitudinal steel bars and tendons, and failure of bearing supports following sudden collapse, as shown in Figure 52.



Figure 51. Ultimate failure of specimen SP-2.



Figure 52. Ultimate failure of specimen SP-3.

8. Conclusions

This study presented a comparison of experimentally measured strains on longitudinal steel bars, stirrups, and tendons placed within two single-span FPP girders and one three-span FPPC girder (SP-1). One of the FPPC girders (SP-2) was designed to simulate the response of that in the interior span of the FPPC girder. The other (i.e., SP-3) was detailed to simulate the response of that in the exterior span of the FPPC girder. A comparison of strain values was presented under both service and ultimate loads. Important results are summarized as follows.

1. Strains within longitudinal steel bars, stirrups, and prestressing tendons were limited well below their corresponding yield limits under service loads. This was observed for all three specimens considered in this study.
2. Under two-point service loads, maximum longitudinal steel strains recorded in FPP were higher than those recorded at corresponding locations in the FPPC girder. This observation was found to be consistent, irrespective of whether the strains were positive or negative. It is worth mentioning that the highest longitudinal steel strains were recorded in specimen SP-3, followed by SP-2 and SP-1, respectively. A similar trend was observed for longitudinal steel strains under four-point service loads on specimen SP-1 and two-point service loads on specimens SP-2 and SP-3.
3. At ultimate loads, longitudinal steel strains (positive and negative) in specimen SP-1 did not reach their yield values. However, corresponding steel strains in specimen SP-2 (i.e., flexure dominated) reached yield values in both positive and negative

directions. Finally, specimen SP-3 (i.e., shear dominated) was able to mobilize yield strain in the positive direction only under ultimate load.

4. For two-point loads limited to service limits, maximum stirrup strains were negligible in all specimens. At ultimate loads, the highest stirrup strains were recorded in specimen SP-1, i.e., three-span girder, within stirrups located at its exterior supports. Nonetheless, those values were lower than the yield strain of stirrups.
5. Under two and four-point service loads, higher tendon strains were usually recorded in specimen SP-3 than those recorded at corresponding locations in specimen SP-1. A similar comparison under similar load levels revealed comparable tendon strains in specimens SP-1 and SP-2.
6. Under ultimate loads, both single-span specimens achieved substantially higher tendon strains than those recorded at the corresponding locations in three-span specimen SP-1. However, maximum tendon strains in specimen SP-3 and exterior span of SP-1 were lower than the yield strain of tendons. This was not true for the interior span of specimen SP-1 and specimen SP-2, where tendon strain reached values significantly higher than yield strains. Nonetheless, the maximum tendon strain recorded within SP-1 was noticeably lower than that recorded in specimen SP-2.

In view of the experimental results obtained, it can be established that single-span girders, detailed to simulate any of the girders in multi-span girders, can induce higher longitudinal steel strains as well as tendon strains. Single-span girders, which are used to simulate the response of multi-span girders can provide safe design guidelines. However, the amount of conservativeness is still a question and further studies are required to verify these results in this context.

Author Contributions: Conceptualization, S.S., A.S., K.C. and P.J.; Formal analysis, M.A.; Funding acquisition, N.A.; Resources, N.A., N.S. and M.A.; Writing—original draft, S.S., A.S., P.J. and Q.H.; Writing—review and editing, S.S., A.S., N.S., K.C., P.J. and Q.H. All authors have read and agreed to the published version of the manuscript.

Funding: This research received no external funding.

Informed Consent Statement: Not applicable.

Acknowledgments: The authors are very thankful to the STECON, Research and Innovation Development Unit for Infrastructure and Rail Transportation Structural System (RIDIR) of Srinakharinwirot University, Thailand and MHPM Co., Ltd. (Guideway Beam Designer) for providing necessary support. Thanks are also extended to Thammasat Research Unit in Infrastructure Inspection and Monitoring, Repair and Strengthening (IIMRS), Thammasat School of Engineering, Faculty of Engineering, Thammasat University Rangsit, Klong Luang, Pathumthani, Thailand, for providing necessary support.

Conflicts of Interest: The authors declare no conflict of interest.

References

1. Liu, X.; Liu, P.; Wang, Q.; Long, L. Feasibility Analysis on Application of Modified Concrete Contains Rubber Powder of Straddle Type Monorail Train Waste Tire. *Procedia Environ. Sci.* **2016**, *31*, 804–811. [[CrossRef](#)]
2. Manoratna, D.A.; Kawata, K.; Yoshida, Y. Environmental Impact and Travel Time Savings of a New Monorail System in Colombo's Commuting Traffic. *Transp. Res. Part D Transp. Environ.* **2017**, *51*, 122–128. [[CrossRef](#)]
3. Kuwabara, T.; Hiraishi, M.; Goda, K.; Okamoto, S.; Ito, A.; Sugita, Y. New Solution for Urban Traffic: Small-Type Monorail System. In Proceedings of the 10th International Conference on Automated People Movers, Orlando, FL, USA, 1–4 May 2005.
4. Yildiz, A.S.; Sivrioglu, S. Semi-Active Vibration Control of Lateral and Rolling Motions for a Straddle Type Monorail Vehicle. *IFAC-PapersOnLine* **2016**, *49*, 279–284. [[CrossRef](#)]
5. Kim, J.T.; Park, J.H.; Hong, D.S.; Park, W.S. Hybrid Health Monitoring of Prestressed Concrete Girder Bridges by Sequential Vibration-Impedance Approaches. *Eng. Struct.* **2010**, *32*, 115–128. [[CrossRef](#)]
6. Ai, D.; Luo, H.; Zhu, H. Numerical and Experimental Investigation of Flexural Performance on Pre-Stressed Concrete Structures Using Electromechanical Admittance. *Mech. Syst. Signal Process.* **2019**, *128*, 244–265. [[CrossRef](#)]
7. Takebayashi, T.; Deeprasertwong, K.; Leung, Y.W. A Full-Scale Destructive Test of a Precast Segmental Box Girder Bridge with Dry Joints and External Tendons. *Open PDF Proc. Inst. Civ. Eng.* **2015**, *104*, 297–315. [[CrossRef](#)]

8. Labia, Y.; Saiidi, M.S.; Douglas, B. Full-Scale Testing and Analysis of 20-Year-Old Pretensioned Concrete Box Girders. *ACI Struct. J.* **1997**, *94*, 471–482. [[CrossRef](#)]
9. Graybeal, B.A. Flexural Behavior of an Ultrahigh-Performance Concrete I-Girder. *J. Bridge Eng.* **2008**, *13*, 602–610. [[CrossRef](#)]
10. Grace, N.; Jensen, E.; Matsagar, V.; Penjendra, P. Performance of an AASHTO Beam Bridge Prestressed with CFRP Tendons. *J. Bridge Eng.* **2013**, *18*, 110–121. [[CrossRef](#)]
11. Van Leeuwen, J.; Adebar, P. Full-Scale Test of Concrete-Steel Hybrid Bridge Girders. *Can. J. Civ. Eng.* **2011**, *25*, 96–103. [[CrossRef](#)]
12. Song, T.; Yang, C.S.W.; Scott, D.W.; Shen, Y.; Li, G. Novel Finite Element Analysis of Curved Concrete Box Girders Using Hybrid Box Elements. *J. Struct. Eng.* **2020**, *147*, 04020284. [[CrossRef](#)]
13. Abid, S.R.; Tayşi, N.; Özakça, M.; Xue, J.; Briseghella, B. Finite Element Thermo-Mechanical Analysis of Concrete Box-Girders. *Structures* **2021**, *33*, 2424–2444. [[CrossRef](#)]
14. Sirisonthi, A.; Suparp, S.; Joyklad, P.; Hussain, Q.; Julphunthong, P. Experimental Study of the Load-Deformation Behaviour of the Precast Post-Tensioned Continuous Girder for Straddle Monorail: Full-Scale Load Test under Service and Ultimate Loading Conditions. *Case Stud. Constr. Mater.* **2021**, *15*, e00666. [[CrossRef](#)]
15. Suparp, S.; Joyklad, P.; Sirisonthi, A.; Hussain, Q. Analysis of Full-Scale Precast Post-Tension (FPP) Girder for Straddle Monorail—Experimental and FEA Study. *Structures* **2022**, *36*, 521–532. [[CrossRef](#)]
16. *ASTM C39/C39M-18*; Standard Test Method for Compressive Strength of Cylindrical Concrete Specimens. ASTM: West Conshohocken, PA, USA, 2020.
17. *ASTM A615/A615M-16*; Standard Specification for Deformed and Plain Carbon-Steel Bars for Concrete Reinforcement. ASTM: West Conshohocken, PA, USA, 2018.
18. *ASTM C109/C109M-21*; Standard Test Method for Compressive Strength of Hydraulic Cement Mortars. ASTM: West Conshohocken, PA, USA, 2021.